Heliyon 9 (2023) e17900

Contents lists available at ScienceDirect

Heliyon

journal homepage: www.cell.com/heliyon

Research article

Modeling the dynamics of COVID-19 in the presence of Delta and Omicron variants with vaccination and non-pharmaceutical interventions

Shikha Saha [a], Amit Kumar Saha [b,*]

[a] Department of Mathematics, Bangladesh University of Engineering and Technology (BUET), Dhaka, 1000, Dhaka, Bangladesh
[b] Department of Mathematics, University of Dhaka, Dhaka, 1000, Dhaka, Bangladesh

ARTICLE INFO

Keywords:
COVID-19
Vaccination
Multiple strain
Delta variant
Omicron variant
Re-infection
Non-pharmaceutical interventions

ABSTRACT

Since its inception in December 2019, many safe and effective vaccines have been invented and approved for use against COVID-19 along with various non-pharmaceutical interventions. But the emergence of numerous SARS-CoV-2 variants has put the effectiveness of these vaccines, and other intervention measures under threat. So it is important to understand the dynamics of COVID-19 in the presence of its variants of concern (VOC) in controlling the spread of the disease. To address these situations and to find a way out of this problem, a new mathematical model consisting of a system of non-linear differential equations considering the original COVID-19 strain with its two variants of concern (Delta and Omicron) has been proposed and formulated in this paper. We then analyzed the proposed model to study the transmission dynamics of this multi-strain model and to investigate the consequences of the emergence of multiple new SARS-CoV-2 variants which are more transmissible than the previous ones. The control reproduction number, an important threshold parameter, is then calculated using the next-generation matrix method. Further, we presented the discussion about the stability of the model equilibrium. It is shown that the disease-free equilibrium (DFE) of the model is locally asymptotic stable when the control reproduction is less than unity. It is also shown that the model has a unique endemic equilibrium (EEP) which is locally asymptotic stable when the control reproduction number is greater than unity. Using the Center Manifold theory it is shown that the model also exhibits the backward bifurcation phenomenon when the control reproduction number is less than unity. Again without considering the re-infection of the recovered individuals, it is proved that the disease-free equilibrium is globally asymptotically stable when the reproduction threshold is less than unity. Finally, numerical simulations are performed to verify the analytic results and to show the impact of multiple new SARS-CoV-2 variants in the population which are more contagious than the previous variants. Global uncertainty and sensitivity analysis has been done to identify which parameters have a greater impact on disease dynamics and control disease transmission. Numerical simulation suggests that the emergence of new variants of concern increases COVID-19 infection and related deaths. It also reveals that a combination of non-pharmaceutical interventions with vaccination programs of new more effective vaccines should be continued to control the disease outbreak. This study also suggests that more doses of vaccine should provide to combat new and deadly variants like Delta and Omicron.

* Corresponding author.
E-mail address: amit92.du@gmail.com (A.K. Saha).

https://doi.org/10.1016/j.heliyon.2023.e17900
Received 20 March 2023; Received in revised form 27 June 2023; Accepted 30 June 2023

Available online 5 July 2023

1. Introduction

The first reported case of COVID-19 was in December 2019 and since then, it has become a global epidemic [1]. As of February 2023, approximately 6.8 million people have died, and approximately 760 million people have been infected which testifies how deadly it is [2]. Before the invention of vaccines, the use of face masks, lock-down, and other non-pharmaceutical interventions and community mitigation strategies (such as: washing and sanitizing hands frequently, and isolation of suspected individuals) were thought to be the effective way to mitigate the disease spread [3,4]. These intervention measures did prove their effectiveness theoretically and mathematically against the pandemic [5,6] but were sometimes insufficient to stop the disease outbreak. So vaccination is thought to be the most effective way to confront this issue and hence vaccinologists worked tirelessly to develop vaccines for preventing COVID-19. At the end of 2020, the first vaccine was approved by World Health Organization (WHO) [7] and it was assumed that vaccination can lead to the end of this pandemic. After that multiple effective vaccines were approved by WHO [7], but the emergence of various new and deadly COVID-19 variants makes it difficult to curtail the disease burden.

It is common for the virus to change over time [8]. In most cases, these changes have little or no impact. But as the variants appear with different forms of mutations, sometimes these changes may affect the level of infectiousness, the severity of the disease, and the vaccine performance [8]. Variants, those that pose an increased risk to public health and the economy, are specified as Variants of Concern (VOCs) and are called so to promote global monitoring and research [9,10]. This feature of viruses is also visible in the case of COVID-19 and till now we have witnessed many variants of COVID-19. Alpha variant (B.1.1.7), having a 75% higher transmission rate than the wild strain, was one of the variants that were listed for SARS-CoV-2 VOC [11]. Delta variant (B.1.617.2), 60% more transmissible than the alpha variant, was another VOC that was first identified in December 2020 and became the most common and dominant one by April 2021 [12]. The last variant, which was listed as a VOC and proved its supremacy over all other variants, was the Omicron variant [13]. It is three times more infectious than the Delta variant [14]. So it is a matter of concern for public health workers and general people as it is seen that the mutated ones may vary in the level of infectiousness and response to the existing vaccines [8].

After the approval of the first vaccine (Pfizer/BioNTech) against COVID-19, mass vaccination programs started in the USA [7, 15]. After that many more vaccines have been approved for use against COVID-19 (Moderna, Janssen J & J, SII/COVIDSHIELD, AstraZeneca/AZD122, Sinopharm, Sinovac-CoronaVac, Bharat Biotech BBV152 COVAXIN, Nuvaxovid) [7]. These vaccines were highly effective against the wild strain but they show varying levels of effectiveness against the new variants like Delta and Omicron [15,16]. Thus the dynamics of COVID-19 in the presence of Delta and Omicron variants will vary significantly and hence it has become necessary for researchers to study the dynamics of COVID-19 in the presence of Delta and Omicron variants to control the disease spread.

In this scenario mathematical model can be used to get insight into the transmission dynamics of COVID-19. Mathematical models can also be analyzed numerically to evaluate the consequences of the new SARS-CoV-2 mutants. There are lots of mathematical models to evaluate the transmission dynamics of COVID-19 [17,6,18–22,16,23,24] and so on. But there are only a few mathematical models to describe the behavior of the COVID-19 wild strain in the presence of its variants of concern [25–28]. Model in [25] considered multiple strains with optimal control theory and waning of immunity. Again model described in [26], evaluated the impact of a new variant for generating more infections, hospitalizations, and deaths. Authors in [27], using a mathematical model, depicted the dynamics of the two strains model under one vaccination regime. They showed the impact of multiple variants and their response to the vaccine and also on developing new infections and deaths. Incorporating vaccination in a two-strain COVID-19 model, authors in [28] showed that a variant would become dominant if it had a higher reproduction number with respect to the other strain. Motivated by the above-mentioned papers, in this paper we formulated and developed a new mathematical model considering the wild strain and its two other variants, Delta and Omicron, to understand the dynamics of COVID-19 transmission. Our goal is to assess the impact of the original strain and its other two variants on developing new infections, hospitalizations, and deaths. Our model is novel in the sense we have considered a three-strain model which has not been investigated before. We have also assessed the effect of the Delta variant and Omicron variant using numerical simulation which is also a new feature of this paper. We have included a compartment for the quarantined individuals in our model as it is known that the most effective way to reduce infection is to isolate the infected individuals. Many studies confirm the re-infection of recovered individuals [29,30] and hence we have considered re-infection of recovered individuals. Global uncertainty and sensitivity analysis is performed in this paper to detect the top-ranked parameters that control the control reproduction number and hence the dynamics of the model.

The entire paper is designed as follows. The formulation of the model is described in section 2. Rigorous and qualitative mathematical analysis of the model has been carried out and the control reproduction number has been calculated in section 3. Vaccine-derived herd immunity threshold has also been calculated in this section. In section 4, numerical results and related discussions are presented. Global uncertainty and sensitivity analysis have also been performed in this section to identify the most influential parameters. Results obtained in theoretical analysis and numerical simulations are summarized in section 5.

2. Materials and methods

2.1. Model formulation

A mathematical model, in the form of a system of non-linear differential equations, has been developed considering the original strain with its two other variants: Delta and Omicron. It has been considered that the wild strain and the mutants have different levels of contagiousness. The compartments: exposed class, pre-symptomatic class, symptomatic class, and asymptomatic class, are

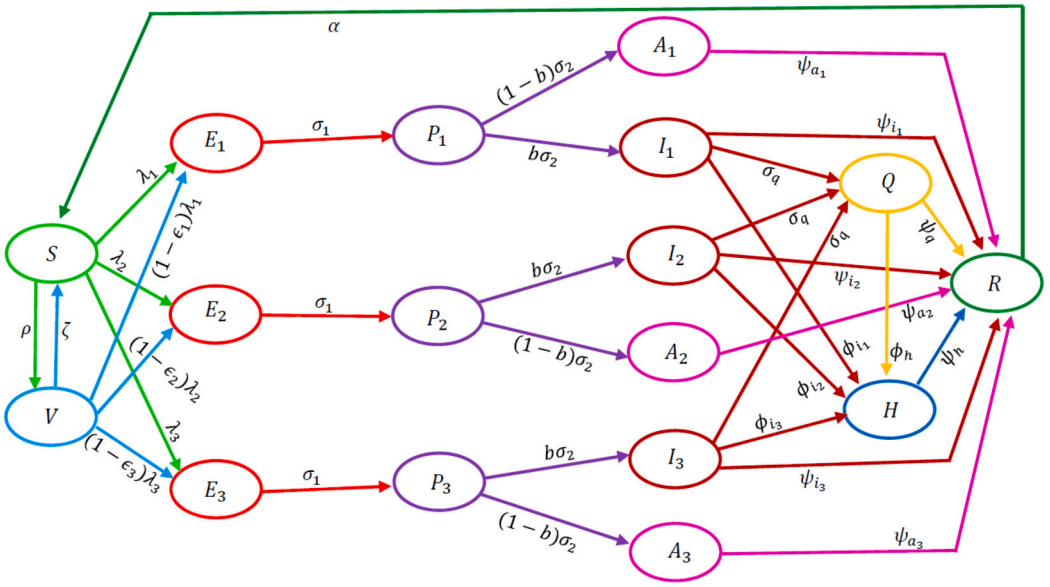

Fig. 1. Schematic diagram of the COVID-19 model (5).

considered separately for each of the strains. The total human population, $N(t)$, is divided into the following mutually exclusive compartments (equation (1)): susceptible (S), vaccinated individuals (V), exposed (E_j), pre-symptomatic (P_j), symptomatic infected (I_j), asymptomatic infected (A_j), quarantined (Q), hospitalized (H) and recovered individuals (R), where $j = 1, 2, 3$, and so we have

$$N(t) = S(t) + V(t) + E_j(t) + P_j(t) + I_j(t) + A_j(t) + Q(t) + H(t) + R(t). \tag{1}$$

Some of the important assumptions in the model formulation are listed below:

Assumption-1: Birth rate (natural recruitment) is not considered.
Assumption-2: Individuals exposed to COVID-19 are unable to infect others.
Assumption-3: Pre-symptomatic and asymptomatic individuals are able to transmit infection.
Assumption-4: Recovered individuals may become susceptible again.
Assumption-5: Preexisting SARS-CoV-2 variants are less contagious than the new variant.

Susceptible individuals acquire infection with the original strain at a rate λ_1, given by

$$\lambda_1 = \frac{\beta_1 (1 - e\, m)(\eta_1 P_1 + I_1 + \theta_1 A_1)}{N}, \tag{2}$$

Again, susceptible individuals acquire infection with the Delta variant at a rate λ_2, given by

$$\lambda_2 = \frac{\beta_2 (1 - e\, m)(\eta_2 P_2 + I_2 + \theta_2 A_2)}{N}, \tag{3}$$

Similarly, susceptible individuals acquire infection with the Omicron variant at a rate λ_3, given by

$$\lambda_3 = \frac{\beta_3 (1 - e\, m)(\eta_3 P_3 + I_3 + \theta_3 A_3)}{N}. \tag{4}$$

Here β_j, $j = 1, 2, 3$ is the effective contact rate of disease transmission for the original strain, Delta strain, and Omicron strain, respectively. It is assumed that people use face masks at a rate m, and e represents face mask efficacy. $0 < \eta_j, \theta_j < 1$ are modification parameters indicating low infectiousness of pre-symptomatic and asymptomatic individuals in the P_j and A_j classes compared to the individuals in the I_j classes, respectively.

Graphical representation of the 3-strain COVID-19 model is shown in Fig. 1. The model is presented in the form of a system of nonlinear differential equations (where a dot represents differentiation with respect to time) as follows:

$$\begin{aligned}
\dot{S} &= \Lambda + \zeta V + \alpha R - \lambda_1 S - \omega_1 \lambda_2 S - \omega_2 \lambda_3 S - \rho S - \mu S,\\
\dot{V} &= \rho S - [(1 - \epsilon_1)\lambda_1 + \omega_1 (1 - \epsilon_2)\lambda_2 + \omega_2 (1 - \epsilon_3)\lambda_3] V - (\zeta + \mu) V,\\
\dot{E}_1 &= \lambda_1 S + (1 - \epsilon_1)\lambda_1 V - (\sigma_1 + \mu) E_1,\\
\dot{P}_1 &= \sigma_1 E_1 - (\sigma_2 + \mu) P_1,
\end{aligned}$$

$$
\begin{aligned}
\dot{I}_1 &= b\sigma_2 P_1 - (\sigma_q + \phi_{i_1} + \psi_{i_1} + \delta_{i_1} + \mu) I_1,\\
\dot{A}_1 &= (1-b)\sigma_2 P_1 - (\psi_{a_1} + \delta_{a_1} + \mu) A_1,\\
\dot{E}_2 &= \omega_1 \lambda_2 S + \omega_1 (1-\epsilon_2) \lambda_2 V - (\sigma_1 + \mu) E_2,\\
\dot{P}_2 &= \sigma_2 E_2 - (\sigma_2 + \mu) P_2,\\
\dot{I}_2 &= b\sigma_2 P_2 - (\sigma_q + \phi_{i_2} + \psi_{i_2} + \delta_{i_2} + \mu) I_2,\\
\dot{A}_2 &= (1-b)\sigma_2 P_2 - (\psi_{a_2} + \delta_{a_2} + \mu) A_2,\\
\dot{E}_3 &= \omega_2 \lambda_3 S + \omega_2 (1-\epsilon_3) \lambda_3 V - (\sigma_1 + \mu) E_3,\\
\dot{P}_3 &= \sigma_1 E_3 - (\sigma_2 + \mu) P_3,\\
\dot{I}_3 &= b\sigma_2 P_3 - (\sigma_q + \phi_{i_3} + \psi_{i_3} + \delta_{i_3} + \mu) I_3,\\
\dot{A}_3 &= (1-b)\sigma_2 P_3 - (\psi_{a_3} + \delta_{a_3} + \mu) A_3,\\
\dot{Q} &= \sigma_q I_1 + \sigma_q I_2 + \sigma_q I_3 - (\phi_q + \psi_q + \delta_q + \mu) Q,\\
\dot{H} &= \phi_{i_1} I_1 + \phi_{i_2} I_2 + \phi_{i_3} I_3 + \phi_q Q - (\psi_h + \delta_h + \mu) H,\\
\dot{R} &= \psi_{i_1} I_1 + \psi_{a_1} A_1 + \psi_{i_2} I_2 + \psi_{a_2} A_2 + \psi_{i_3} I_3 + \psi_{a_3} A_3 + \psi_q Q + \psi_h H - (\alpha + \mu) R.
\end{aligned} \tag{5}
$$

In the model (5), Λ is the recruitment rate of individuals. ρ represents the rate at which susceptible individuals are vaccinated. Vaccinated population further moves to the susceptible class due to the loss of acquired immunity from vaccine at a rate ζ. Individuals exposed to the original strain of COVID-19 move to the pre-symptomatic stage at a rate σ_1. Pre-symptomatic individuals gain infection at a rate σ_2. Among the infected individuals who show the symptoms of COVID-19 are generated at a proportion b. As we know, individuals infected with COVID-19 may not show the symptoms of the disease but at the same time, they are capable of infecting others. We have considered a class for these asymptomatic individuals as they play an important role in the transmission dynamics of COVID-19. Among the infected individuals who do not show the symptoms of COVID-19 are generated at a proportion $1-b$. σ_q is the rate at which infected individuals are sent to quarantine. Symptomatic infected individuals in the I_1, I_2 and I_3 classes are hospitalized at a rate ϕ_{i_1}, ϕ_{i_2} and ϕ_{i_3}, respectively. Individuals in the I_1, A_1, I_2, A_2, I_3 and A_3 classes recover from COVID-19 at a rate ψ_{i_1}, ψ_{a_1}, ψ_{i_2}, ψ_{a_2}, ψ_{i_3} and ψ_{a_3}, respectively. COVID-19 induced death rates for individuals in the I_1, A_1, I_2, A_2, I_3 and A_3 classes are δ_{i_1}, δ_{a_1}, δ_{i_2}, δ_{a_2}, δ_{i_3} and δ_{a_3}, respectively. Recovered individuals become susceptible again at a reduced rate α. $\omega_2 > \omega_1 > 1$ are modification parameters indicating high infectiousness of the Omicron variant and Delta variant with respect to the original strain. μ represents the natural death rate.

3. Mathematical analysis of the model

3.1. Local asymptotic stability of the DFE

From the COVID-19 model (5), the disease-free equilibrium, $\mathcal{E}_0$, is obtained as

$$
\mathcal{E}_0 = \left(S^*, V^*, E_j^*, P_j^*, I_j^*, A_j^*, Q^*, H^*, R^*\right) = \left(\frac{\Lambda k_2}{k_1 k_2 - \zeta\rho}, \frac{\Lambda\rho}{k_1 k_2 - \zeta\rho}\, 0, 0, 0, 0, 0, 0, 0\right). \tag{6}
$$

The asymptotic stability of the DFE can be established using the next-generation operator method [31,32] on the system (5). For the system (5), using the notation of [32], the next generation matrices for the new infection terms and remaining transfer terms, denoted by F and V respectively, are given by

$$
F = \begin{pmatrix}
0 & \eta_1\beta_1\mathcal{F}_1 & \beta_1\mathcal{F}_1 & \theta_1\beta_1\mathcal{F}_1 & 0 & 0 & 0 & 0 & 0 & 0 & 0 & 0\\
0 & 0 & 0 & 0 & 0 & 0 & 0 & 0 & 0 & 0 & 0 & 0\\
0 & 0 & 0 & 0 & 0 & 0 & 0 & 0 & 0 & 0 & 0 & 0\\
0 & 0 & 0 & 0 & 0 & 0 & 0 & 0 & 0 & 0 & 0 & 0\\
0 & 0 & 0 & 0 & 0 & \eta_2\beta_2\mathcal{F}_2 & \beta_2\mathcal{F}_2 & \theta_2\beta_2\mathcal{F}_2 & 0 & 0 & 0 & 0\\
0 & 0 & 0 & 0 & 0 & 0 & 0 & 0 & 0 & 0 & 0 & 0\\
0 & 0 & 0 & 0 & 0 & 0 & 0 & 0 & 0 & 0 & 0 & 0\\
0 & 0 & 0 & 0 & 0 & 0 & 0 & 0 & 0 & 0 & 0 & 0\\
0 & 0 & 0 & 0 & 0 & 0 & 0 & 0 & 0 & \eta_3\beta_3\mathcal{F}_3 & \beta_3\mathcal{F}_3 & \theta_3\beta_3\mathcal{F}_3\\
0 & 0 & 0 & 0 & 0 & 0 & 0 & 0 & 0 & 0 & 0 & 0\\
0 & 0 & 0 & 0 & 0 & 0 & 0 & 0 & 0 & 0 & 0 & 0\\
0 & 0 & 0 & 0 & 0 & 0 & 0 & 0 & 0 & 0 & 0 & 0
\end{pmatrix},
$$

$$V = \begin{pmatrix} k_3 & 0 & 0 & 0 & 0 & 0 & 0 & 0 & 0 & 0 & 0 & 0 \\ -\sigma_1 & k_4 & 0 & 0 & 0 & 0 & 0 & 0 & 0 & 0 & 0 & 0 \\ 0 & -b\sigma_2 & k_5 & 0 & 0 & 0 & 0 & 0 & 0 & 0 & 0 & 0 \\ 0 & -(1-b)\sigma_2 & 0 & k_6 & 0 & 0 & 0 & 0 & 0 & 0 & 0 & 0 \\ 0 & 0 & 0 & 0 & k_3 & 0 & 0 & 0 & 0 & 0 & 0 & 0 \\ 0 & 0 & 0 & 0 & -\sigma_1 & k_4 & 0 & 0 & 0 & 0 & 0 & 0 \\ 0 & 0 & 0 & 0 & 0 & -b\sigma_2 & k_7 & 0 & 0 & 0 & 0 & 0 \\ 0 & 0 & 0 & 0 & 0 & -(1-b)\sigma_2 & 0 & k_8 & 0 & 0 & 0 & 0 \\ 0 & 0 & 0 & 0 & 0 & 0 & 0 & 0 & k_3 & 0 & 0 & 0 \\ 0 & 0 & 0 & 0 & 0 & 0 & 0 & 0 & -\sigma_1 & k_4 & 0 & 0 \\ 0 & 0 & 0 & 0 & 0 & 0 & 0 & 0 & 0 & -b\sigma_2 & k_9 & 0 \\ 0 & 0 & 0 & 0 & 0 & 0 & 0 & 0 & 0 & -(1-b)\sigma_2 & 0 & k_{10} \end{pmatrix},$$

where,

$$\mathcal{F}_1 = (1-em)\frac{S^*+(1-\epsilon_1)V^*}{N^*},\ \mathcal{F}_2 = (1-em)\frac{S^*+(1-\epsilon_2)V^*}{N^*},\ \mathcal{F}_3 = (1-em)\frac{S^*+(1-\epsilon_3)V^*}{N^*},$$

$$k_1 = \rho+\mu,\ k_2 = \zeta+\mu,\ k_3 = \sigma_1+\mu,\ k_4 = \sigma_2+\mu,\ k_5 = \sigma_q+\phi_{i_1}+\psi_{i_1}+\delta_{i_1}+\mu,\ k_6 = \psi_{a_1}+\delta_{a_1}+\mu,$$

$$k_7 = \sigma_q+\phi_{i_2}+\psi_{i_2}+\delta_{i_2}+\mu,\ k_8 = \psi_{a_2}+\delta_{a_2}+\mu,\ k_9 = \sigma_q+\phi_{i_3}+\psi_{i_3}+\delta_{i_3}+\mu,\ k_{10} = \psi_{a_3}+\delta_{a_3}+\mu,$$

$$k_{11} = \phi_q+\psi_q+\delta_q+\mu,\ k_{12} = \psi_h+\delta_h+\mu,\ k_{13} = \alpha+\mu.$$

Following the approach described in [33,34], it can be shown that the control reproduction number, denoted by $\mathcal{R}_c$, is given by

$$\mathcal{R}_c = \rho(F V^{-1}) = \max\left\{\mathcal{R}_1,\ \mathcal{R}_2,\ \mathcal{R}_3\right\}, \tag{7}$$

where, ρ represents the spectral radius of the next generation matrix $F V^{-1}$ and

$$\mathcal{R}_1 = \frac{\eta_1\beta_1\mathcal{F}_1\sigma_1}{k_3k_4}+\frac{\beta_1\mathcal{F}_1 b\sigma_2\sigma_1}{k_3k_4k_5}+\frac{\theta_1\beta_1\mathcal{F}_1(1-b)\sigma_1\sigma_2}{k_3k_4k_6}. \tag{8}$$

$$\mathcal{R}_2 = \frac{\eta_2\beta_2\mathcal{F}_2\sigma_1}{k_3k_4}+\frac{\beta_2\mathcal{F}_2 b\sigma_1\sigma_2}{k_3k_4k_7}+\frac{\theta_2\beta_2\mathcal{F}_2(1-b)\sigma_1\sigma_2}{k_3k_4k_8}. \tag{9}$$

$$\mathcal{R}_3 = \frac{\eta_3\beta_3\mathcal{F}_3\sigma_1}{k_3k_4}+\frac{\beta_3\mathcal{F}_3 b\sigma_1\sigma_2}{k_3k_4k_9}+\frac{\theta_3\beta_3\mathcal{F}_3(1-b)\sigma_1\sigma_2}{k_3k_4k_{10}}. \tag{10}$$

Consequently, using Theorem 2 of [32] the following result can be established.

Lemma 1. *The DFE of the COVID-19 model (5), given by (6), is locally-asymptotically stable (LAS) if $\mathcal{R}_c < 1$, and unstable if $\mathcal{R}_c > 1$.*

The threshold quantity $\mathcal{R}_c$, given by (7), represents the average number of secondary infections that one infected case can produce in a completely susceptible population. Lemma 1 implies that, in general, when $\mathcal{R}_c$ is less than one, a small influx of infected individuals into the population would not generate a large epidemic and hence the disease will be eradicated in time. However, in the subsection 3.3 we will see that the disease may still exist even when $\mathcal{R}_c < 1$.

3.2. Derivation of vaccine-induced herd immunity threshold to reduce the spread of COVID-19

In this subsection, we will compute the minimum number of populations that should be brought under vaccination to achieve herd immunity. To do this, we will follow the procedure as described in [35]. From equations (8), (9), and (10) we get,

$$\mathcal{R}_1 = (1-em)\left[\left(\frac{\eta_1\beta_1\sigma_1}{k_3k_4}+\frac{\beta_1 b\sigma_2\sigma_1}{k_3k_4k_5}+\frac{\theta_1\beta_1(1-b)\sigma_1\sigma_2}{k_3k_4k_6}\right)\left(\frac{S^*}{N^*}+\frac{V^*}{N^*}-\epsilon_1\frac{V^*}{N^*}\right)\right]. \tag{11}$$

$$\mathcal{R}_2 = (1-em)\left[\left(\frac{\eta_2\beta_2\sigma_1}{k_3k_4}+\frac{\beta_2 b\sigma_1\sigma_2}{k_3k_4k_7}+\frac{\theta_2\beta_2(1-b)\sigma_1\sigma_2}{k_3k_4k_8}\right)\left(\frac{S^*}{N^*}+\frac{V^*}{N^*}-\epsilon_2\frac{V^*}{N^*}\right)\right]. \tag{12}$$

$$\mathcal{R}_3 = (1-em)\left[\left(\frac{\eta_3\beta_3\sigma_1}{k_3k_4}+\frac{\beta_3 b\sigma_1\sigma_2}{k_3k_4k_9}+\frac{\theta_3\beta_3(1-b)\sigma_1\sigma_2}{k_3k_4k_{10}}\right)\left(\frac{S^*}{N^*}+\frac{V^*}{N^*}-\epsilon_3\frac{V^*}{N^*}\right)\right]. \tag{13}$$

At the DFE, we have

$$N^* = S^*+V^* = \frac{\Lambda(k_2+\rho)}{k_1k_2-\zeta\rho}. \tag{14}$$

Using expression (14), equations (11), (12), and (13) become

$$\mathcal{R}_1 = (1-em)\left[\frac{\eta_1\beta_1\sigma_1}{k_3k_4}\left(1-\epsilon_1\frac{V^*}{N^*}\right)+\frac{\beta_1 b\sigma_2\sigma_1}{k_3k_4k_5}\left(1-\epsilon_1\frac{V^*}{N^*}\right)+\frac{\theta_1\beta_1(1-b)\sigma_1\sigma_2}{k_3k_4k_6}\left(1-\epsilon_1\frac{V^*}{N^*}\right)\right]. \tag{15}$$

$$\mathcal{R}_2 = (1-em)\left[\frac{\eta_2\beta_2\sigma_1}{k_3k_4}\left(1-\epsilon_2\frac{V^*}{N^*}\right)+\frac{\beta_2 b\sigma_1\sigma_2}{k_3k_4k_7}\left(1-\epsilon_2\frac{V^*}{N^*}\right)+\frac{\theta_2\beta_2(1-b)\sigma_1\sigma_2}{k_3k_4k_8}\left(1-\epsilon_2\frac{V^*}{N^*}\right)\right]. \tag{16}$$

$$\mathcal{R}_3 = (1-em)\left[\frac{\eta_3\beta_3\sigma_1}{k_3k_4}\left(1-\epsilon_3\frac{V^*}{N^*}\right)+\frac{\beta_3 b\sigma_1\sigma_2}{k_3k_4k_9}\left(1-\epsilon_3\frac{V^*}{N^*}\right)+\frac{\theta_3\beta_3(1-b)\sigma_1\sigma_2}{k_3k_4k_{10}}\left(1-\epsilon_3\frac{V^*}{N^*}\right)\right]. \tag{17}$$

Now using the expressions of S^*, V^*, and N^*, from equations (6) and (14), in equations (15), (16), and (17) we get

$$\mathcal{R}_1 = (1-em)\left[\frac{\eta_1\beta_1\sigma_1}{k_3k_4}\left(1-\epsilon_1\frac{\rho}{k_2+\rho}\right)+\frac{\beta_1 b\sigma_2\sigma_1}{k_3k_4k_5}\left(1-\epsilon_1\frac{\rho}{k_2+\rho}\right)+\frac{\theta_1\beta_1(1-b)\sigma_1\sigma_2}{k_3k_4k_6}\left(1-\epsilon_1\frac{\rho}{k_2+\rho}\right)\right]. \tag{18}$$

$$\mathcal{R}_2 = (1-em)\left[\frac{\eta_2\beta_2\sigma_1}{k_3k_4}\left(1-\epsilon_2\frac{\rho}{k_2+\rho}\right)+\frac{\beta_2 b\sigma_1\sigma_2}{k_3k_4k_7}\left(1-\epsilon_2\frac{\rho}{k_2+\rho}\right)+\frac{\theta_2\beta_2(1-b)\sigma_1\sigma_2}{k_3k_4k_8}\left(1-\epsilon_2\frac{\rho}{k_2+\rho}\right)\right]. \tag{19}$$

$$\mathcal{R}_3 = (1-em)\left[\frac{\eta_3\beta_3\sigma_1}{k_3k_4}\left(1-\epsilon_3\frac{\rho}{k_2+\rho}\right)+\frac{\beta_3 b\sigma_1\sigma_2}{k_3k_4k_9}\left(1-\epsilon_3\frac{\rho}{k_2+\rho}\right)+\frac{\theta_3\beta_3(1-b)\sigma_1\sigma_2}{k_3k_4k_{10}}\left(1-\epsilon_3\frac{\rho}{k_2+\rho}\right)\right]. \tag{20}$$

To find an expression for the vaccine-derived herd immunity threshold, we will use the expression for the basic reproduction number which is obtained by setting $V^* = 0$ and $\epsilon_j = 0$. Again, suppose that

$$f_v = \frac{V^*}{N^*}, \tag{21}$$

where f_v represents the proportion of individuals who are fully vaccinated. Thus, using the expression (21) in equations (18), (19), and (20), we obtain

$$\mathcal{R}_1 = (1-em)\left[\frac{\eta_1\beta_1\sigma_1}{k_3k_4}\left(1-\epsilon_1 f_v\right)+\frac{\beta_1 b\sigma_2\sigma_1}{k_3k_4k_5}\left(1-\epsilon_1 f_v\right)+\frac{\theta_1\beta_1(1-b)\sigma_1\sigma_2}{k_3k_4k_6}\left(1-\epsilon_1 f_v\right)\right]. \tag{22}$$

$$\mathcal{R}_2 = (1-em)\left[\frac{\eta_2\beta_2\sigma_1}{k_3k_4}\left(1-\epsilon_2 f_v\right)+\frac{\beta_2 b\sigma_1\sigma_2}{k_3k_4k_7}\left(1-\epsilon_2 f_v\right)+\frac{\theta_2\beta_2(1-b)\sigma_1\sigma_2}{k_3k_4k_8}\left(1-\epsilon_2 f_v\right)\right]. \tag{23}$$

$$\mathcal{R}_3 = (1-em)\left[\frac{\eta_3\beta_3\sigma_1}{k_3k_4}\left(1-\epsilon_3 f_v\right)+\frac{\beta_3 b\sigma_1\sigma_2}{k_3k_4k_9}\left(1-\epsilon_3 f_v\right)+\frac{\theta_3\beta_3(1-b)\sigma_1\sigma_2}{k_3k_4k_{10}}\left(1-\epsilon_3 f_v\right)\right]. \tag{24}$$

Let $\mathcal{R}_{0j} = \mathcal{R}_j|_{V^*=0,\epsilon_j=0} \quad j = 1, 2, 3$

Setting $\mathcal{R}_1 = 1$ in (22) and solving for f_v, the herd immunity threshold for the model with the original strain only can be obtained as

$$f_v = \frac{1}{\epsilon_1}\left(1-\frac{1}{\mathcal{R}_{01}}\right). \tag{25}$$

Similarly, setting $\mathcal{R}_2 = 1$ in (23) and solving for f_v, the herd immunity threshold for the model with the original strain and the Delta variant can be obtained as

$$f_v = \frac{1}{\epsilon_2}\left(1-\frac{1}{\mathcal{R}_{02}}\right). \tag{26}$$

Finally, setting $\mathcal{R}_3 = 1$ in (24) and solving for f_v, the herd immunity threshold for the model with the original strain and the Delta and Omicron variants can be obtained as

$$f_v = \frac{1}{\epsilon_3}\left(1-\frac{1}{\mathcal{R}_{03}}\right). \tag{27}$$

In general, equations (25), (26), and (27) can be written as

$$f_v = \frac{1}{\epsilon_j}\left(1-\frac{1}{\mathcal{R}_{0j}}\right). \tag{28}$$

It follows from (28) that $\mathcal{R}_c < 1$ if $f_v > \frac{1}{\epsilon_j}\left(1-\frac{1}{\mathcal{R}_{0j}}\right)$ and hence the disease can be eliminated. Lemma 1 can be re-stated in terms of the herd immunity threshold as follows.

Lemma 2. *The DFE of the COVID-19 model (5), is locally-asymptotically stable (LAS) if* $f_v > \frac{1}{\epsilon_j}\left(1-\frac{1}{\mathcal{R}_{0j}}\right)$ *and unstable if* $f_v < \frac{1}{\epsilon_j}\left(1-\frac{1}{\mathcal{R}_{0j}}\right)$.

3.3. Endemic equilibrium point (EEP) and existence of backward bifurcation

Setting the left-hand side of the model (5) equal to zero, we get the following system of equations:

$$\begin{aligned}
0 &= \Lambda + \zeta V^* + \alpha R^* - \lambda_1 S^* - \lambda_2 S^* - \lambda_3 S^* - k_1 S^*,\\
0 &= \rho S^* - \left[(1-\epsilon_1)\lambda_1 + (1-\epsilon_2)\lambda_2 + (1-\epsilon_3)\lambda_3\right] V^* - k_2 V^*,\\
0 &= \lambda_1 S^* + (1-\epsilon_1)\lambda_1 V^* - k_3 E_1^*,\\
0 &= \sigma_1 E_1^* - k_4 P_1^*,\\
0 &= b\sigma_2 P_1^* - k_5 I_1^*,\\
0 &= (1-b)\sigma_2 P_1^* - k_6 A_1^*,\\
0 &= \lambda_2 S^* + (1-\epsilon_2)\lambda_2 V^* - k_3 E_2^*,\\
0 &= \sigma_2 E_2^* - k_4 P_2^*,\\
0 &= b\sigma_2 P_2^* - k_7 I_2^*,\\
0 &= (1-b)\sigma_2 P_2^* - k_8 A_2^*,\\
0 &= \lambda_3 S + (1-\epsilon_3)\lambda_3 V^* - k_3 E_3^*,\\
0 &= \sigma_1 E_3^* - k_4 P_3^*,\\
0 &= b\sigma_2 P_3^* - k_9 I_3^*,\\
0 &= (1-b)\sigma_2 P_3^* - k_{10} A_3^*,\\
0 &= \sigma_q I_1^* + \sigma_q I_2^* + \sigma_q I_3^* - k_{11} Q^*,\\
0 &= \phi_{i_1} I_1^* + \phi_{i_2} I_2^* + \phi_{i_3} I_3^* + \phi_q Q^* - k_{12} H^*,\\
0 &= \psi_{i_1} I_1^* + \psi_{a_1} A_1^* + \psi_{i_2} I_2^* + \psi_{a_2} A_2^* + \psi_{i_3} I_3^* + \psi_{a_3} A_3^* + \psi_q Q^* + \psi_h H^* - k_{13} R^*,
\end{aligned} \tag{29}$$

3.3.1. Endemic equilibria and backward bifurcation for the model with the original strain only

First, suppose that there is only the original strain. Then we can consider $E_2^* = P_2^* = I_2^* = A_2^* = E_3^* = P_3^* = I_3^* = A_3^* = 0$. Let $\mathcal{E}_1 = (S^*, V^*, E_1^*, P_1^*, I_1^*, A_1^*, 0, 0, 0, 0, 0, 0, 0, 0, Q^*, H^*, R^*)$ be any arbitrary equilibrium of the model (5) when there is only the original strain and hence equation (2) can be written as

$$\lambda_1^* = \frac{\beta_1 (1 - e\,m)(\eta_1 P_1^* + I_1^* + \theta_1 A_1^*)}{N^*} \tag{30}$$

be the force of infection at steady-state. Therefore, from the system (29) we have,

$$\begin{aligned}
S^* &= \frac{\Lambda k_3 \left\{(1-\epsilon_1)\lambda_1^* + k_2\right\}}{M_{1_1} \lambda_1^{*^2} + M_{2_1} \lambda_1^* + M_{3_1}}, \quad V^* = \frac{\rho \Lambda k_3}{M_{1_1} \lambda_1^{*^2} + M_{2_1} \lambda_1^* + M_{3_1}}, \quad E_1^* = \frac{\lambda_1^* (M_{4_1} \lambda_1^* + M_{5_1})}{M_{1_1} \lambda_1^{*^2} + M_{2_1} \lambda_1^* + M_{3_1}},\\
P_1^* &= B_{p_1} E_1^*, \quad I_1^* = B_{i_1} E_1^*, \quad A_1^* = B_{a_1} E_1^*, \quad Q^* = B_{q_1} E_1^*, \quad H^* = B_{h_1} E_1^*, \quad R^* = B_{r_1} E_1^*,
\end{aligned} \tag{31}$$

where,

$$\begin{aligned}
&B_{p_1} = \frac{\sigma_1}{k_4}, \; B_{i_1} = \frac{b\sigma_2}{k_5}, \; B_{a_1} = \frac{(1-b)\sigma_2}{k_6}, \; B_{q_1} = \frac{b\sigma_1\sigma_2\sigma_q}{k_4 k_5 k_{11}}, \; B_{h_1} = \frac{\phi_{i_1} B_{i_1} + \phi_q B_{q_1}}{k_{12}},\\
&B_{r_1} = \frac{\psi_{i_1} B_{i_1} + \psi_{a_1} B_{a_1} + \psi_q B_{q_1} + \psi_h B_{h_1}}{k_{13}},\\
&M_{1_1} = (1-\epsilon_1)(k_3 + \alpha B_{r_1}), \; M_{2_1} = (1-\epsilon_1) k_1 k_3 + k_2 (1 - \alpha B_{r_1}) - \alpha B_{r_1} (1-\epsilon_1)\rho, \; M_{3_1} = -\eta\rho k_2, \; M_{4_1} = \Lambda(1-\epsilon_1),\\
&M_{5_1} = \Lambda k_2 + \Lambda(1-\epsilon_1)\rho.
\end{aligned}$$

Substituting (31) into (30) gives

$$\lambda_1^* = \frac{\beta_1 (1 - e\,m)(\eta_1 B_{p_1} + B_{i_1} + \theta_1 B_{a_1}) \left(M_{4_1} \lambda_1^{*^2} + M_{5_1} \lambda_1^*\right)}{\Lambda k_3 \left\{(1-\epsilon_1)\lambda_1^* + k_2\right\} + \rho \Lambda k_3 + B_{c_1} \left(M_{4_1} \lambda_1^{*^2} + M_{5_1} \lambda_1^*\right)}, \tag{32}$$

where,

$$B_{c_1} = 1 + B_{p_1} + B_{i_1} + B_{a_1} + B_{q_1} + B_{h_1} + B_{r_1}.$$

After some algebraic calculation, the following polynomial equation in terms of λ_1^* can be obtained from equation (32) as

Table 1
Numerical values of the parameters for the model (5).

Parameter	Baseline Values	Units	References
Λ	10000	Day^{-1}	Assumed
$\beta_1, \beta_2, \beta_3$	0.35, 0.39, 0.45	Day^{-1}	Fitted
m	0.4	-	Fitted
e	0.5	-	[5]
η_1, η_2, η_3	0.75, 0.75, 0.75	-	Fitted
$\theta_1, \theta_2, \theta_3$	0.85, 0.85, 0.85	-	Fitted
ω_1, ω_2	2.25, 7.5	-	Fitted
ρ, ζ, α	0.78, 0.05, 0.003	Day^{-1}	Fitted
$\epsilon_1, \epsilon_2, \epsilon_3$	0.85, 0.75, 0.8	-	Fitted
$\sigma_1, \sigma_2, \sigma_q$	0.2, 0.25 0.12	Day^{-1}	Estimated from [36]
b and $1-b$	0.45, 0.55	-	Assumed
$\phi_{i_1}, \phi_{i_2}, \phi_{i_3}$ and ϕ_q	0.12, 0.17, 0.12, 0.15	Day^{-1}	Fitted
$\psi_{i_1}, \psi_{i_2}, \psi_{i_3}, \psi_{a_1},$	0.14, 0.12, 0.13, 0.17,	Day^{-1}	Estimated from [36]
$\psi_{a_2}, \psi_{a_3}, \psi_q$ and ψ_h	0.15, 0.19, 0.2, 0.15,	Day^{-1}	Estimated from [36]
$\delta_{i_1}, \delta_{i_2}, \delta_{i_3}, \delta_{a_1},$	0.007, 0.009, 0.006, 0.001	Day^{-1}	Estimated from [36]
$\delta_{a_2}, \delta_{a_3}, \delta_q$ and δ_h	0.001, 0.003, 0.004, 0.006	Day^{-1}	Estimated from [36]
μ	0.00004	Day^{-1}	[6]

$$\lambda_1^* \left\{ P_{2_1} \lambda_1^{*^2} + P_{1_1} \lambda_1^* + P_{0_1} \right\} = 0, \tag{33}$$

where,

$$\begin{aligned} P_{2_1} &= B_{c_1} M_{4_1}, \\ P_{1_1} &= B_{c_1} M_{5_1} + \Lambda k_3 (1-\epsilon_1) - M_{4_1} \beta_1 (1-e\,m)(\eta_1 B_{p_1} + B_{i_1} + \theta_1 B_{a_1}), \\ P_{0_1} &= \Lambda k_3 (\rho + k_2)(1 - \mathcal{R}_1). \end{aligned}$$

Out of the three roots, the root $\lambda_1^* = 0$, of (33), corresponds to the DFE $\mathcal{E}_0$. Equation (33) says that the non-zero equilibria of the model satisfy

$$f(\lambda_1^*) = P_{2_1} \lambda_1^{*^2} + P_{1_1} \lambda_1^* + P_{0_1} = 0, \tag{34}$$

so that the quadratic (34) can be analyzed for the possibility of multiple equilibria. If multiple non-zero equilibria exist then backward bifurcation may occur.

Endemic equilibria: From the above, we see that the coefficient P_{2_1} is always positive and P_{0_1} is positive if $\mathcal{R}_1$ is less than one and P_{0_1} is negative if $\mathcal{R}_1$ is greater than one. Hence, we have the following result.

Theorem 1. *The model* (5) *with the original strain only has*

(i) a unique endemic equilibrium if $P_{0_1} < 0$ *(i.e.,* $\mathcal{R}_1 > 1$*),*
(ii) a unique endemic equilibrium if $P_{1_1} < 0$*, and* $P_{0_1} = 0$ *or* $P_{1_1}^2 - 4 P_{2_1} P_{0_1} = 0$*,*
(iii) two endemic equilibria if $P_{1_1} < 0$*,* $P_{0_1} > 0$ *(i.e.,* $\mathcal{R}_1 < 1$*) and* $P_{1_1}^2 - 4 P_{2_1} P_{0_1} > 0$*,*
(iv) *no endemic equilibrium otherwise.*

Condition-i of Theorem 1 says that the model with the original strain only has a unique endemic equilibrium when $\mathcal{R}_1 > 1$. Using the parameter values as given in Table 1 with $\alpha = 0$ it can be shown that $\mathcal{R}_1 > 1$ which implies there exists a unique endemic equilibrium. Again from the expressions of a_1 and b_1, we get $a_1 < 0$ and $b_1 > 0$. Thus according to the Center Manifold theory [37,32,38], this unique endemic equilibrium is locally asymptotically stable when $\mathcal{R}_1 > 1$. Hence, we have the following theorem.

Theorem 2. *The model* (5) *with the original strain only and with* $\alpha = 0$ *has a unique endemic equilibrium which is locally asymptotically stable when* $\mathcal{R}_1 > 1$.

Backward bifurcation analysis: Condition-iii of Theorem 1, implies the possibility of having two endemic equilibria (co-existence of locally-asymptotically stable DFE with a locally asymptotically stable endemic equilibrium) whenever $\mathcal{R}_1 < 1$ and hence implies the occurrence of backward bifurcation phenomenon. Since there exists a stable endemic equilibrium with the stable DFE, the condition $\mathcal{R}_1 < 1$ is no longer sufficient (although necessary) for disease elimination. The significance of the existence of backward bifurcation is that COVID-19 will persist in the community even when $\mathcal{R}_1 < 1$. Thus, disease elimination will depend not only on the condition $\mathcal{R}_1 < 1$ but also on the initial sizes of the state variables of the model. Now, using the parameter values as given in Table 1 with $\rho = 0.002$, $\zeta = 0.000004$ we have $P_{1_1} < 0$ and $P_{0_1} > 0$ indicating the possibility of the existence of backward bifurcation. Now this will be explained using the Center Manifold theory [37,32,38]. The procedure is described in Appendix A. The

graphical representation of the backward bifurcation of the model (5) with the original strain only is shown in Fig. 2. We claim the following result.

Theorem 3. *The model (5) with the original strain only exhibits backward bifurcation whenever the coefficients a_1 and b_1, given by (A.3), are positive.*

3.3.2. Endemic equilibria and backward bifurcation for the model with the original strain and the Delta variant

Now we will consider the case when there exists the Delta variant with the original strain. Here, we will consider that the transmission rate of the Delta variant is higher than the existing one. That is, $\beta_2 > \beta_1$. In this case, we will not consider any term and equation involving the Omicron variant. Then we have the following theorem.

Theorem 4. *Suppose that $\beta_2 > \beta_1$. Then $E_1^* = P_1^* = I_1^* = A_1^* = 0$.*

Proof. We will prove this by the method of contradiction as described in [26]. So suppose that $\beta_2 > \beta_1$ and also suppose that $E_1^* = P_1^* = I_1^* = A_1^* \neq 0$. Then from the 4th and 8th equations of system (29) we have

$$P_2^* = \frac{P_1^* E_2^*}{E_1^*}, \tag{35}$$

Similarly,

$$I_2^* = \frac{I_1^* E_2^*}{E_1^*}, \tag{36}$$

And

$$A_2^* = \frac{A_1^* E_2^*}{E_1^*}. \tag{37}$$

Thus using equations (35), (36) and (37), the 7th equation of system (29) becomes

$$(\sigma_1 + \mu) E_2^* = \lambda_2 \left\{ S^* + (1 - \epsilon_2) V^* \right\}. \tag{38}$$

Hence, from equation (38), we obtain

$$(\sigma_1 + \mu) E_2^* > \frac{E_2^*}{n E_1^*} \left\{ S^* + (1 - \epsilon_2) V^* \right\} \left(\beta_1 \eta_1 P_1^* + \beta_1 I_1^* + \beta_1 \theta_1 A_1^* \right). \tag{39}$$

Thus, equation (39) implies

$$(\sigma_1 + \mu) E_1^* > \left\{ S^* + (1 - \epsilon_2) V^* \right\} \lambda_1. \tag{40}$$

Hence equation (40) contradicts the 3rd equation of the system (29). This implies $E_1^* = P_1^* = I_1^* = A_1^* = 0$ holds if $\beta_2 > \beta_1$.

The detailed calculation of the endemic equilibria and the existence of backward bifurcation for the original model with the Delta variant has been provided in Appendix C.

Endemic equilibria: Depending on the sign of the coefficients P_{0_2}, P_{1_2}, and P_{2_2} given by (C.5) and considering the equation (C.6), we have the following result.

Theorem 5. *The model (5) with the original strain and the Delta variant has*

(i) a unique endemic equilibrium if $P_{0_2} < 0$ (i.e., $\mathcal{R}_2 > 1$),
(ii) a unique endemic equilibrium if $P_{1_2} < 0$, and $P_{0_2} = 0$ or $P_{1_2}^2 - 4 P_{2_2} P_{0_2} = 0$,
(iii) two endemic equilibria if $P_{1_2} < 0$, $P_{0_2} > 0$ (i.e., $\mathcal{R}_2 < 1$) and $P_{1_2}^2 - 4 P_{2_2} P_{0_2} > 0$,
(iv) no endemic equilibrium otherwise.

Using the parameter values as given in Table 1 with $\alpha = 0$ it can be shown that $\mathcal{R}_2 > 1$ which implies the existence of a unique endemic equilibrium. Also from the expressions of a_2 and b_2, we get $a_2 < 0$ and $b_2 > 0$. Thus according to the Center Manifold theory [37,32,38], this unique endemic equilibrium is locally asymptotically stable when $\mathcal{R}_2 > 1$.
Hence, we have the following theorem.

Theorem 6. *The model (5) with the original strain and the Delta variant and with $\alpha = 0$ has a unique endemic equilibrium which is locally asymptotically stable when $\mathcal{R}_2 > 1$.*

Backward bifurcation analysis: Now, using the parameter values as given in Table 1 with $\rho = 0.002$, $\zeta = 0.000004$ we have $P_{1_2} < 0$ and $P_{0_2} > 0$. Thus Condition-iii of Theorem 5 says that the model with the original strain and the Delta variant has two endemic equilibria which indicate the possibility of the occurrence of backward bifurcation. The procedure is described in Appendix C. We claim the following result.

Theorem 7. *The model* (5) *with the original strain and the Delta variant exhibits backward bifurcation whenever the coefficients* a_2, *and* b_2 *given by* (C.7) *are positive.*

3.3.3. Endemic equilibria and backward bifurcation for the model with the original strain and the Delta and Omicron variants

Finally, we will consider the case when there exists both the Omicron variant and the Delta variant with the original strain.

Theorem 8. *Suppose that* $\beta_3 > \beta_2 > \beta_1$. *Then* $E_1^* = P_1^* = I_1^* = A_1^* = E_2^* = P_2^* = I_2^* = A_2^* = 0$.

Proof. Using the same procedure as described in Theorem 4, it can be shown that if we consider $\beta_3 > \beta_2 > \beta_1$, then $E_1^* = P_1^* = I_1^* = A_1^* = E_2^* = P_2^* = I_2^* = A_2^* = 0$.

The detailed calculation of the endemic equilibria and the existence of backward bifurcation for the original model with the Delta and Omicron variants has been provided in Appendix D.

Endemic equilibria: Depending on the sign of the coefficients P_{0_3}, P_{1_3}, and P_{2_3} given by (D.5) and considering the equation (D.6), we have the following theorem.

Theorem 9. *The model* (5) *with the original strain and the Delta and Omicron variants has*

(i) a unique endemic equilibrium if $P_{0_3} < 0$ *(i.e.,* $\mathcal{R}_3 > 1$*),*
(ii) a unique endemic equilibrium if $P_{1_3} < 0$, *and* $P_{0_3} = 0$ *or* $P_{1_3}^2 - 4P_{2_3}P_{0_3} = 0$,
(iii) two endemic equilibria if $P_{1_3} < 0$, $P_{0_3} > 0$ *(i.e.,* $\mathcal{R}_3 < 1$*) and* $P_{1_3}^2 - 4P_{2_3}P_{0_3} > 0$,
(iv) no endemic equilibrium otherwise.

Using the parameter values as given in Table 1 with $\alpha = 0$ it can be shown that $\mathcal{R}_3 > 1$ which implies the existence of a unique endemic equilibrium. Also from the expressions of a_3 and b_3, we get $a_3 < 0$ and $b_3 > 0$. Thus according to the Center Manifold theory [37,32,38], this unique endemic equilibrium is locally asymptotically stable when $\mathcal{R}_3 > 1$.
Hence, we have the following theorem.

Theorem 10. *The model* (5) *with the original strain and the Delta and Omicron variants and with* $\alpha = 0$ *has a unique endemic equilibrium which is locally asymptotically stable when* $\mathcal{R}_3 > 1$.

Backward bifurcation analysis: Now, using the parameter values as given in Table 1 with $\rho = 0.002$, $\zeta = 0.000004$ we have $P_{1_3} < 0$ and $P_{0_3} > 0$. Thus Condition-iii of Theorem 9 says that the model with the original strain and the Delta and Omicron variants has two endemic equilibria which indicate the possibility of the existence of backward bifurcation. The procedure is described in Appendix D. We claim the following result.

Theorem 11. *The model* (5) *with the original strain and the Delta and Omicron variants exhibit backward bifurcation whenever the coefficients* a_3, *and* b_3 *given by* (D.7) *are positive.*

3.4. Global stability of DFE when there is no re-infection

Define the region

$$D = \left\{ \left(S^*, V^*, E_j^*, P_j^*, I_j^*, A_j^*, Q^*, H^*, R^* \right) \in \mathbb{R}_+^{17} : N \leq \frac{\Lambda}{\mu} \right\}. \tag{41}$$

We claim the following.

Lemma 3. *The region* D, *given by equation* (41), *is positively-invariant and attracting with respect to the model* (5).

Proof. Using the same procedure as described in [6] and performing some calculations, it can be easily shown that the region D is positively-invariant and attracting.

Now, we claim the following theorem.

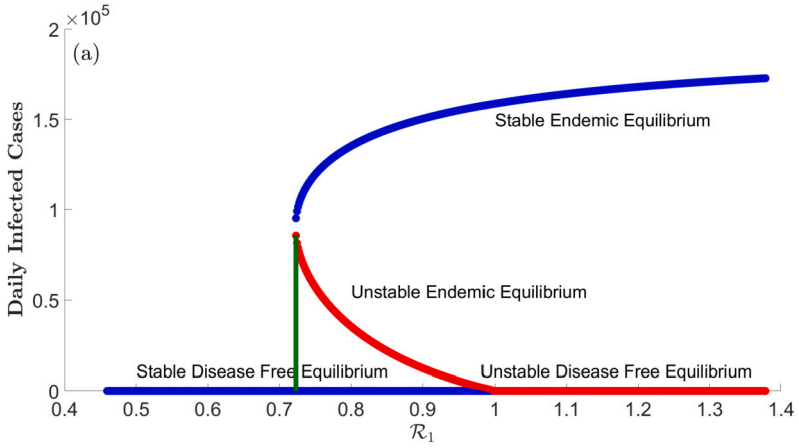

Fig. 2. Backward bifurcation of the model (5) with the original strain only. Parameter values are used as given in Table 1 with $\rho = 0.002$, $\zeta = 0.000004$.

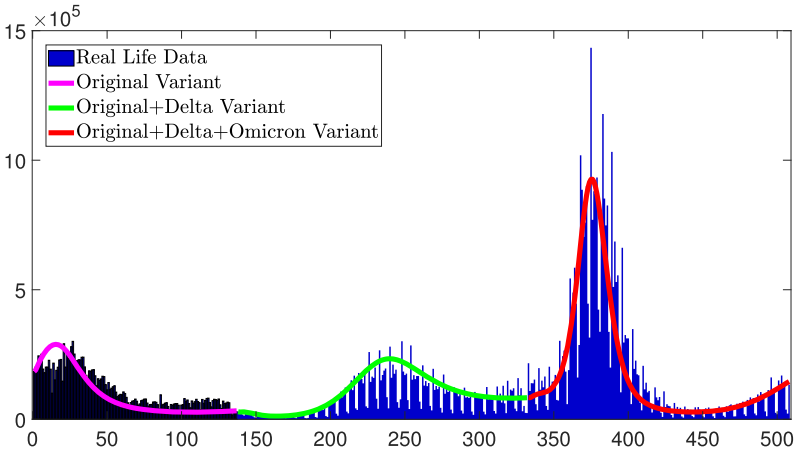

Fig. 3. Validation of the model (5), showing the model's output for the daily infected cases vs the daily confirmed cases for the United States starting from December 13, 2020, to May 23, 2022, using baseline parameter values given in Table 1.

Theorem 12. *The DFE of the COVID-19 model* (5) *with no re-infection, given by* $\mathcal{E}_0$*, is globally asymptotically stable (GAS) whenever* $\mathcal{R}_c \leq 1$.

The detailed calculation of the proof of this theorem is provided in Appendix B.

4. Results and discussions

Numerical simulations of the COVID-19 original strain with the Delta and Omicron variants in the form of model (5) are performed and results have been discussed in this section. To perform numerical simulations we consider that the new variant is more infectious than the previous ones and we use the parameter values as given in Table 1. Values of parameters with the same biological meaning are taken from some already-existing articles. Some parameter values are obtained by fitting the daily infected cases of the USA with our model solution using the MATLAB fminsearchbnd function. Some values are estimated from available COVID-19 data and sources from published articles. Other parameter values are assumed.

4.1. Model validation

In this section, real data of daily infected cases for the entire USA population [2] is shown using bar diagram (blue colored) and in the same figure window we have drawn the infected class of our model to compare our model with the real-time data and hence to verify the reliability of our model. Fig. 3 presents the real-time data vs the model outcome which tests the validity of our model.

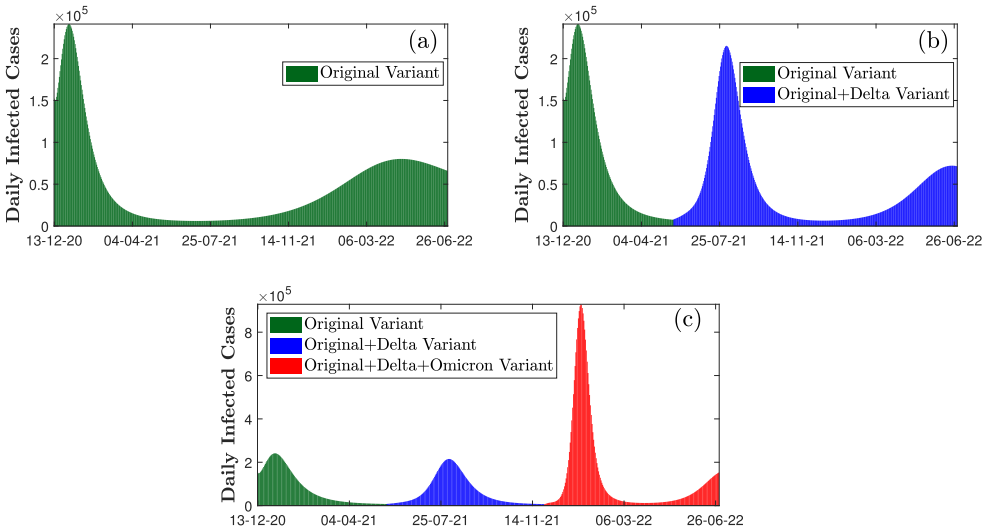

Fig. 4. Simulation of the model (5) showing the effect of variants of concern (Delta and Omicron) on daily infected cases for the model (5). Fig. 4 (a) shows the simulation result when there is only the original strain. Fig. 4 (b) shows the simulation result when there exists the Delta variant with the original strain. Fig. 4 (c) shows the simulation result when there exist both the Delta and Omicron variants with the original strain.

4.2. Effect of the emergence of new Sars-CoV-2 variants

Now we will discuss the effect of the emergence of new SARS-CoV-2 variants (Delta and Omicron) on daily infected cases, daily hospitalized cases, and daily death cases. For this, we will consider three cases:

Case 1: Existence of the original strain only.
Case 2: Existence of the original strain with the Delta variant.
Case 3: Existence of the original strain with the Delta and Omicron variants.

Fig. 4 depicts the effect of the emergence of new variants of concern on the daily infected cases. Fig. 4 (a) shows that when there is no other variant other than the original one, the maximum number of daily infected cases is 240893 which occurs on January 2, 2021 After that, the number of daily infected cases starts decreasing. Again from August 9, 2021, the number of daily infected cases starts increasing and we witness a second wave where the peak value (80152) is much smaller than the previous peak. But considering the existence of the Delta variant with the original one (Fig. 4 (b)), we see that the second wave starts faster (May 20, 2021) than the previous case (Fig. 4 (a)) and here the peak value is 215331 which occurs on August 4, 2021, and is almost close to the first peak for the original strain. This figure also shows a third wave which starts on January 10, 2022, and here the peak value (72106) is much smaller than the peaks observed in the first wave and the second wave respectively. Again, considering both the Delta variant and Omicron variant with the original strain (Fig. 4 (c)), it is seen that the third wave emerges faster (November 29, 2021) than the previous case (Fig. 4 (b)) and here the peak value is (928719) which occurs on January 12, 2022, and is much much larger than the peak occurred in the third wave of the second case. This figure also exhibits the starting of a fourth wave. These results suggest that during the time period considered in this simulation, total infected cases increase by 14% due to the presence of the Delta variant. Cumulative infected cases almost doubled when both the Delta and Omicron variants are present. Similarly, during this time period cumulative death cases increase by 5.4% due to the emergence of the Delta variant (Fig. 6 (b)), and death cases increase by 19% if both the Delta and Omicron variants appear (Fig. 6 (c)). The same pattern is observed for daily hospitalized cases (Fig. 5). Thus, from these discussions, it is clear that the number of infected cases, hospitalized cases, and death cases increase due to the presence of Delta and Omicron variants.

4.3. Global sensitivity and uncertainty analysis

Now to identify which parameters have a greater impact on the dynamics of our model, we perform global uncertainty and sensitivity analysis [39,40]. For this, we applied the method discussed in [41] to our model. In this paper, we have sampled 37 parameters of our model using Latin hyperbolic sampling and considering uniform distribution. Parameters with PRCC values greater or equal to 0.5 and less or equal to -0.5 are considered to be highly correlated with the response function [42]. Performing the global uncertainty and sensitivity analysis for the symptomatic infected class (I_1) of the model with the original strain only and the model parameters (Fig. 7 (a)), we see that the top-ranked parameters those can affect the dynamics of the model (5) with the original strain only are $\beta_1, \sigma_1, \sigma_2, \epsilon_1, \psi_{i_1}, \psi_{a_1}, \phi_{i_1}, \zeta, \rho, e, m$. Again considering $\mathcal{R}_1$ as the response function (Fig. 7 (b)), it is seen that parameters those affect the dynamics of the model (5) with original variant only are $\beta_1, \sigma_2, \epsilon_1, \psi_{i_1}, \psi_{h_1}, \phi_{i_1}, \rho, m$. Again performing the global uncertainty and sensitivity analysis for the symptomatic infected class (I_2) of the model with the original strain and the Delta

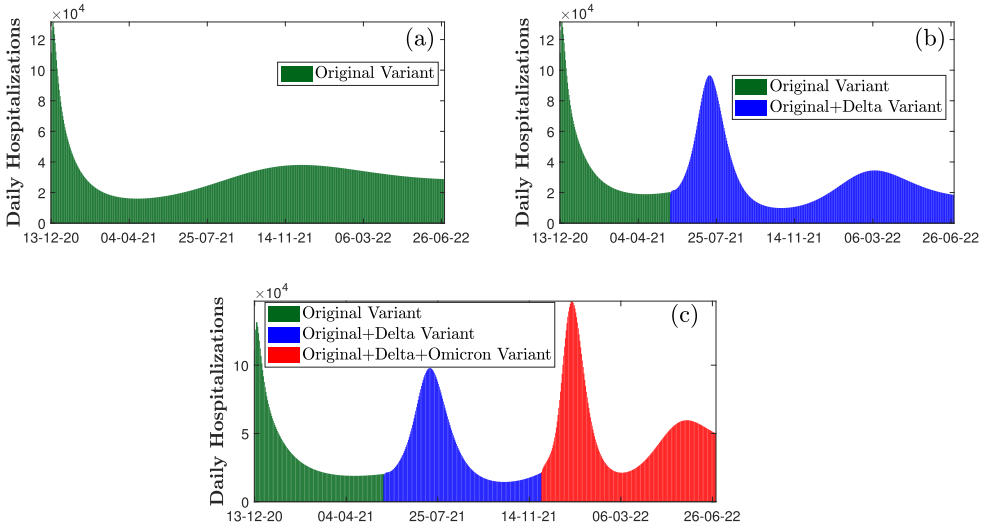

Fig. 5. Simulation of the model (5) showing the effect of variants of concern (Delta and Omicron) on daily hospitalized cases for the model (5). Fig. 5 (a) shows the simulation result when there is only the original strain. Fig. 5 (b) shows the simulation result when there exists the Delta variant with the original strain. Fig. 5 (c) shows the simulation result when there exist both the Delta and Omicron variants with the original strain.

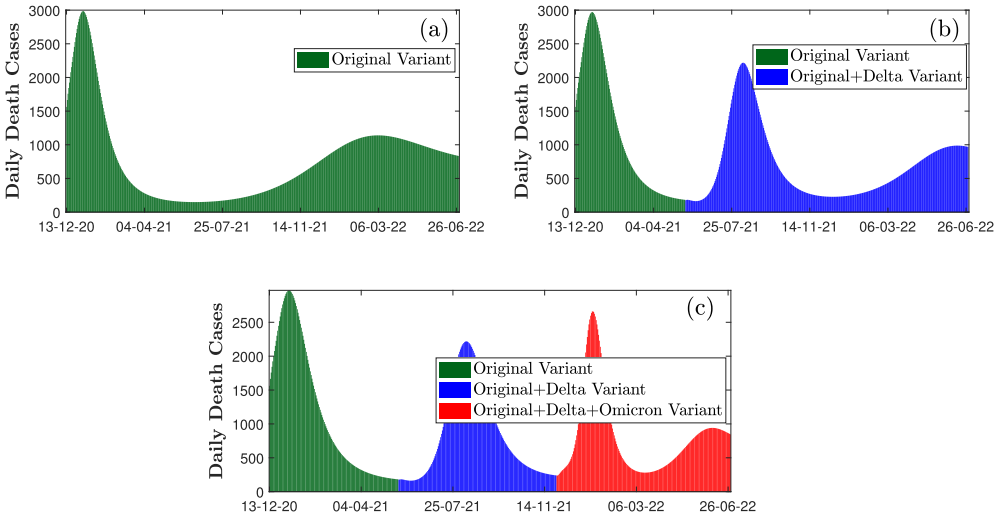

Fig. 6. Simulation of the model (5) showing the effect of variants of concern (Delta and Omicron) on daily death cases for the model (5). Fig. 6 (a) shows the simulation result when there is only the original strain. Fig. 6 (b) shows the simulation result when there exists the Delta variant with the original strain. Fig. 6 (c) shows the simulation result when there exist both the Delta and Omicron variants with the original strain.

variant and the model parameters (Fig. 8 (a)), it is observed that the top-ranked parameters are ω_1, β_2, σ_1, σ_2, ϵ_2, ψ_{i_2}, ϕ_{i_2}, ζ, ρ, e, m those can control the dynamics of the model. Again considering $\mathcal{R}_2$ as the response function (Fig. 8 (b)), it is seen that parameters that affect the dynamics of the model (5) with the original strain and the Delta variant are β_2, σ_2, ϵ_2, ψ_{i_2}, ψ_{a_2}, ϕ_{i_2}, ρ, m. Similarly calculating the global sensitivity analysis for the symptomatic infected class (I_3) of the model with the original strain and the Delta and Omicron variants and the model parameters (Fig. 9 (a)), it is observed that parameters that can affect the model dynamics are ω_2, β_3, σ_1, σ_2, ϵ_3, ζ, ρ, e, m. Parameters β_2, ϵ_3, ψ_{i_3}, ψ_{a_3}, ϕ_{i_3}, ρ, m are found as the top-ranked parameters while performing global uncertainty analysis for the response function $\mathcal{R}_3$ and the model parameters (Fig. 9 (b)).

4.4. Effect of vaccination

The impact of vaccination coverage is assessed by simulating the model (5) with different values of vaccination rate (ρ). For this, we have considered BNT162b2 vaccine against the original strain of COVID-19 and its two other variants: Delta and Omicron. As it is observed that due to the change in genetic pattern, new variants of concern are emerging very frequently, and hence vaccine efficacy (ϵ_j) may change over time. The results obtained from the simulation are depicted in Fig. 10. From this figure, a significant decrease in daily infected cases, daily hospitalized cases, and daily deaths are observed when the vaccination rate is increased. For

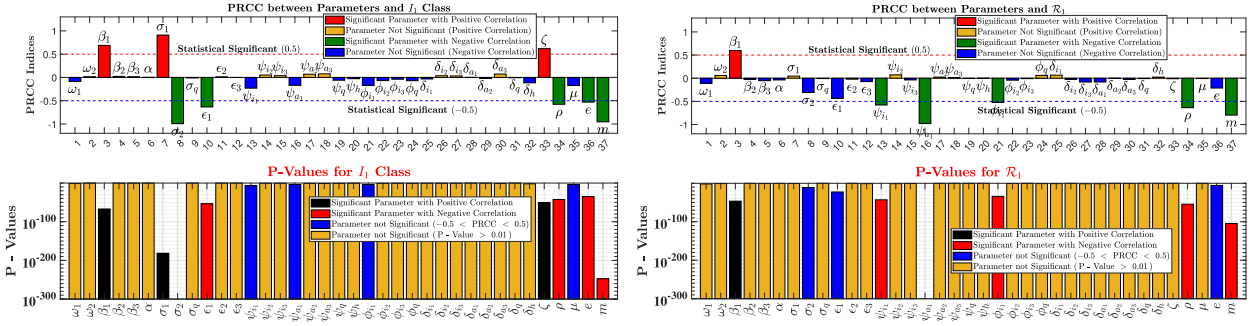

(a) (b)

Fig. 7. Global uncertainty and sensitivity analysis of the system of differential equations (5). Fig. 7 (a) shows the partial rank correlation coefficient and P-value among the model parameters and the response function I_1. Fig. 7 (b) shows the partial rank correlation coefficient and P-value among the model parameters and the response function $\mathcal{R}_1$.

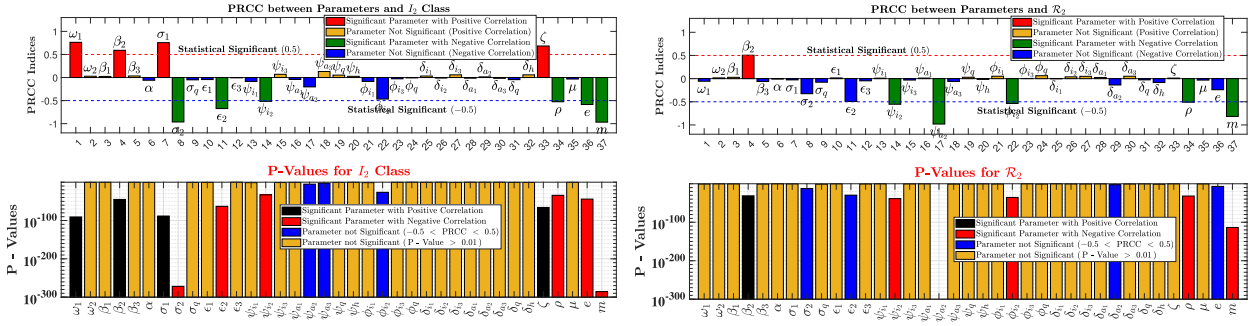

(a) (b)

Fig. 8. Global uncertainty and sensitivity analysis of the system of differential equations (5). Fig. 8 (a) shows the partial rank correlation coefficient and P-value among the model parameters and the response function I_2. Fig. 8 (b) shows the partial rank correlation coefficient and P-value among the model parameters and the response function $\mathcal{R}_2$.

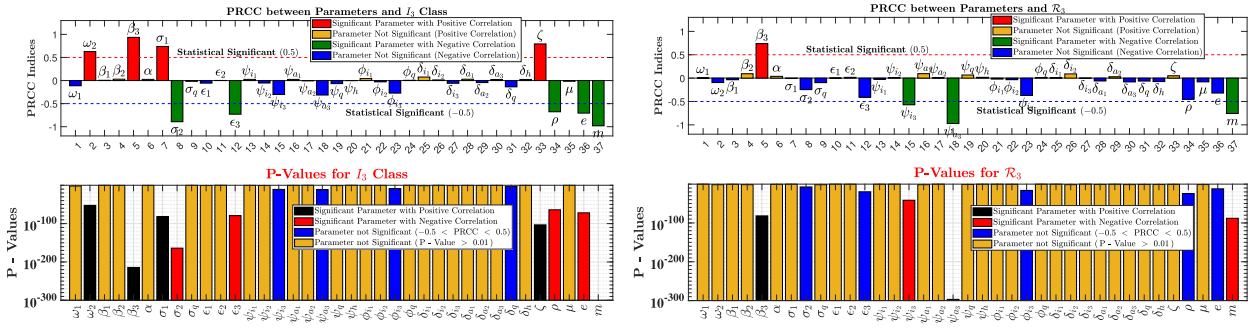

(a) (b)

Fig. 9. Global uncertainty and sensitivity analysis of the system of differential equations (5). Fig. 9 (a) shows the partial rank correlation coefficient and P-value among the model parameters and the response function I_3. Fig. 9 (b) shows the partial rank correlation coefficient and P-value among the model parameters and the response function $\mathcal{R}_3$.

example, Fig. 10 (a) shows that if there is no immunization program, the peak value of the daily infected cases is 1577690. If 25% of the population are vaccinated the peak of the daily infected cases decreases by 41%. The peak value of daily infected cases further decreases by 17% when 50% of the population is vaccinated. The figure further depicts a 12% decrease in the peak value of daily infected cases when 90% of the population is vaccinated. Similar trends are observed in daily hospitalized cases and daily death cases with an increasing rate of vaccine coverage. As a whole Fig. 10 shows that the peak of daily infected cases, daily hospitalized cases, and daily death cases can be decreased with an increase in the vaccination rate. To assess the combined effect of vaccine coverage and vaccine efficacy, contour plot of the control reproduction number of the model (5) as a function of vaccine efficacy (ϵ_j) and the fraction of the population fully vaccinated (f_v) is presented in Fig. 11. Fig. 11 (a) shows that when there exists only the original

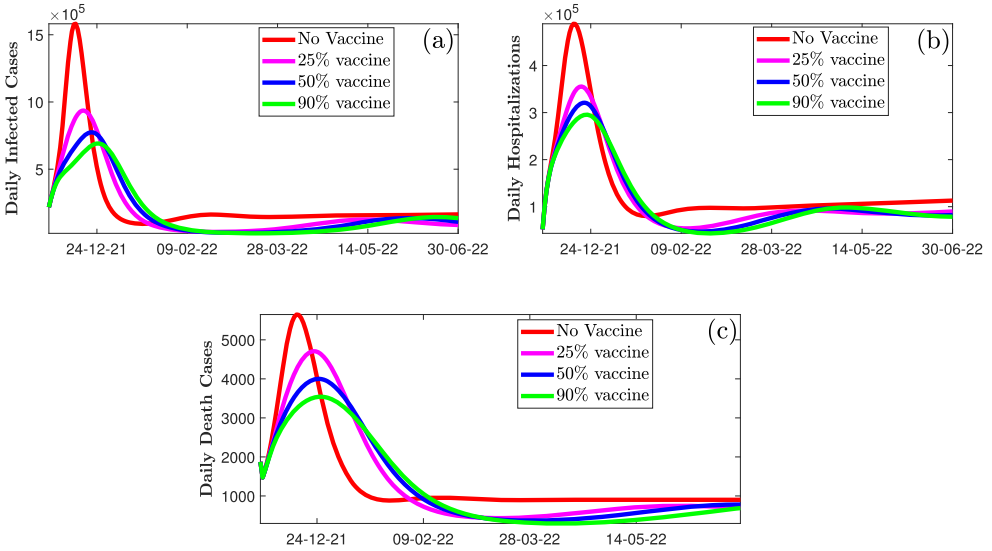

Fig. 10. Simulation of the model (5) showing the effect of vaccine coverage (ρ) on daily infected cases, daily hospitalized cases, and daily deaths. Fig. 10 (a) shows the daily infected cases for different percentages of vaccine coverage. Fig. 10 (b) shows the daily hospitalized cases for different percentages of vaccine coverage. Fig. 10 (c) shows the daily deaths for different percentages of vaccine coverage.

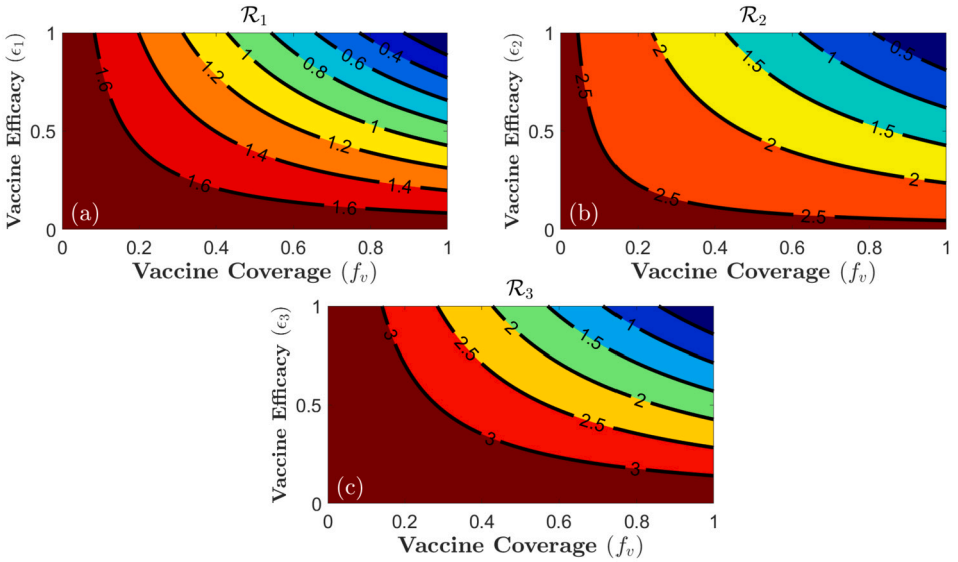

Fig. 11. Contour plot of the control reproduction number of the model (5) as a function of vaccine coverage (f_v) and vaccine efficacy (ϵ_j). Fig. 11 (a) presents the contour plot of $\mathcal{R}_1$ of the model (5) for the original strain. Fig. 11 (b) presents the contour plot of $\mathcal{R}_2$ of the model (5) for the original strain with Delta variant. Fig. 11 (c) presents the contour plot of $\mathcal{R}_3$ of the model (5) for the original strain with the Delta and Omicron variants.

strain, herd immunity can be achieved if 65% population is vaccinated with vaccines having 70% efficacy. Fig. 11 (b) shows that when there exists the Delta variant with the original strain, herd immunity can be achieved if 75% population is vaccinated with vaccines having 85% efficacy. Fig. 11 (c) shows that when there exists both the Delta variant and Omicron variant with the original strain, herd immunity can be achieved if 80% population is vaccinated with vaccines having 90% efficacy.

4.5. Effect of mask coverage

The impact of mask coverage (m) and mask efficacy (e) is also evaluated by simulating the model (5) with different values of mask coverage and mask efficacy. Here we have considered three types of masks of different efficacy: cloth mask (30% efficacy), surgical mask (70% efficacy), and N95 mask (95% efficacy). The results are presented in Fig. 12. These results show that the peak of the daily infected cases, daily hospitalized cases, and daily death cases decrease remarkably with the increase in mask coverage particularly if the moderately effective surgical masks and highly effective N95 masks are used even when vaccine coverage is kept

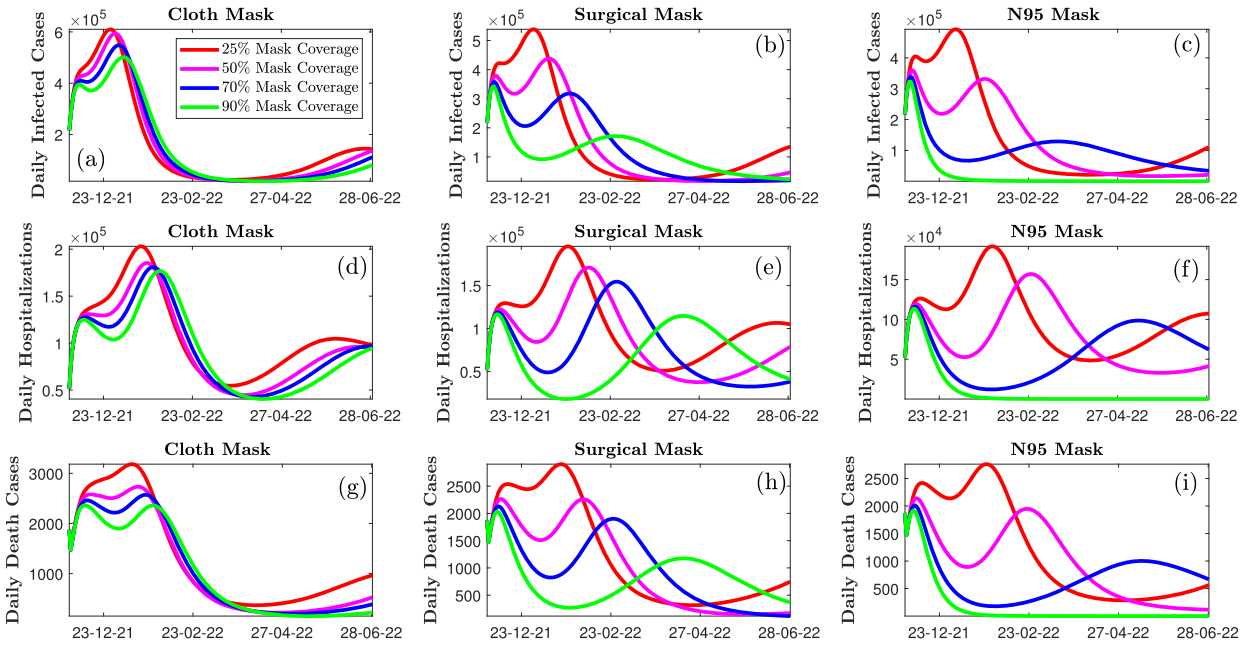

Fig. 12. Simulation of the model (5) showing the effect of mask quality (e) and mask coverage (m). Fig. 12 (a), (d), and (g) show the daily infected cases, daily hospitalized cases, and daily deaths when cloth mask is used with different mask coverage rate. Fig. 12 (b), (e), and (h) show the daily infected cases, daily hospitalized cases, and daily deaths when surgical mask is used with different mask coverage rate. Fig. 12 (c), (f), and (i) show the daily infected cases, daily hospitalized cases, and daily deaths when N95 mask is used with different mask coverage rate.

at the baseline value. For instance, Fig. 12 (b) and (c) show a 20% and 35% decrease in the peak of daily infected cases when 50% of the total population wear surgical masks and N95 masks respectively. The figure also shows that if 70% of the total population uses face masks of the above-mentioned two types, the peak of the daily infected cases again decreases by 30% and 60% respectively. This figure does not show any significant decrease in the peak of daily infected cases in the case of less effective cloth masks. Thus these figures show that in reducing the peak of daily cases, N95 mask quality is proved to be highly effective which is followed by surgical masks. Our results also show that a 45% increase in the baseline value of surgical mask coverage proves to be more effective than a 25% increase in the baseline value of N95 mask coverage. Similarly, we can say that ensuring maximum number of people in the community wearing a moderate mask is more important than fewer people wearing highly effective face masks. These analyses also suggest that fewer people reluctant to use a highly effective N95 mask are less harmful than more people reluctant to use a moderately effective surgical mask.

Simulations are also carried out to assess the combined effect of mask coverage and mask efficacy using contour plot of the control reproduction number of the model (5) as a function of mask coverage and mask efficacy and is presented in Fig. 13. Fig. 13 (a) shows that when there exists only the original strain, COVID-19 can be eliminated if 50% population uses face masks having 3% efficacy. Fig. 13 (b) shows that when there exists the Delta variant with the original strain, COVID-19 can be eliminated if 65% population uses face masks having 85% efficacy. Fig. 13 (c) shows that when there exists both the Delta and Omicron variants with the original strain, COVID-19 can be eliminated if 0% population uses face masks having 95% efficacy.

4.6. Combined effect of vaccination and mask coverage

Numerical simulation of the model (5) is also carried out to assess the combined effect of mask coverage and vaccine coverage on the peak of daily infected cases, daily hospitalized cases, and daily deaths. The simulation results are presented in Fig. 14. Fig. 14 (a) shows that when no vaccine is implemented and 25% individuals use face masks, the peak of the daily infected case is 1478910. But when 25% of the individual is vaccinated and 50% individual use face masks the peak of the daily infected cases decreases by 61%. Further, a 40% decrease is observed when 50% of the individual is vaccinated and 70% individual use face masks. Again, a 52% decrease is observed when 90% of the individual is vaccinated and 90% individual use face masks. Similar trends are observed for the daily hospitalized case (Fig. 14 (b)) and for the daily death cases (Fig. 14 (c)). This simulation suggests that more reduction in the peak of daily infected cases can be achieved if both the vaccine coverage rate and mask coverage rate are increased simultaneously.

5. Conclusion

To understand the transmission dynamics of COVID-19 in the presence of new variants, a mathematical model considering Delta and Omicron variants with the original strain was proposed and formulated. In this work, our focus was mainly on assessing the impact of introducing new SARS-CoV-2 variants: Delta and Omicron whose contagiousness were assumed to be greater than the

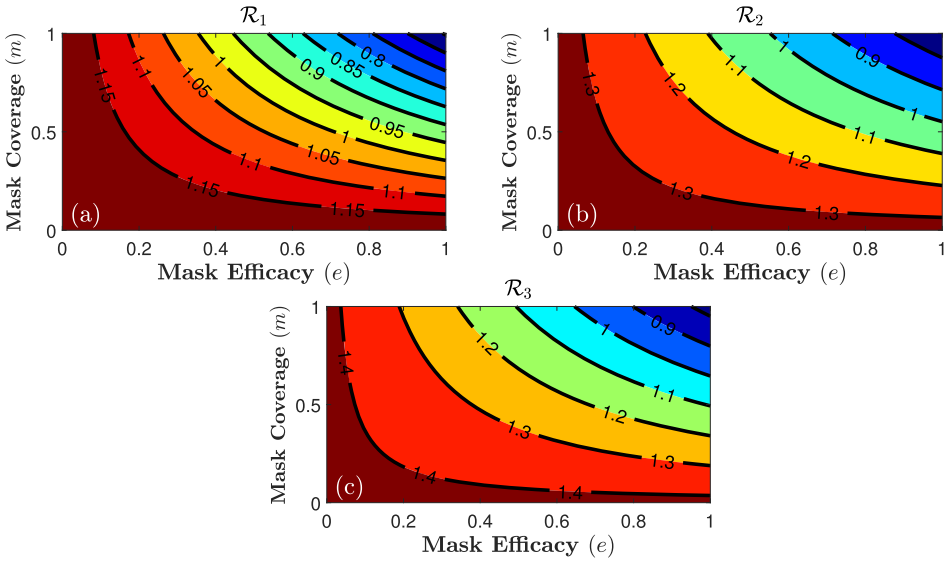

Fig. 13. Contour plot of the control reproduction number of the model (5) as a function of mask coverage (m) and mask efficacy (e). Fig. 13 (a) presents the contour plot of $\mathcal{R}_1$ of the model (5) for the original strain. Fig. 11 (b) presents the contour plot of $\mathcal{R}_2$ of the model (5) for the original strain with Delta variant. Fig. 11 (c) presents the contour plot of $\mathcal{R}_3$ of the model (5) for the original strain with Delta and Omicron variant.

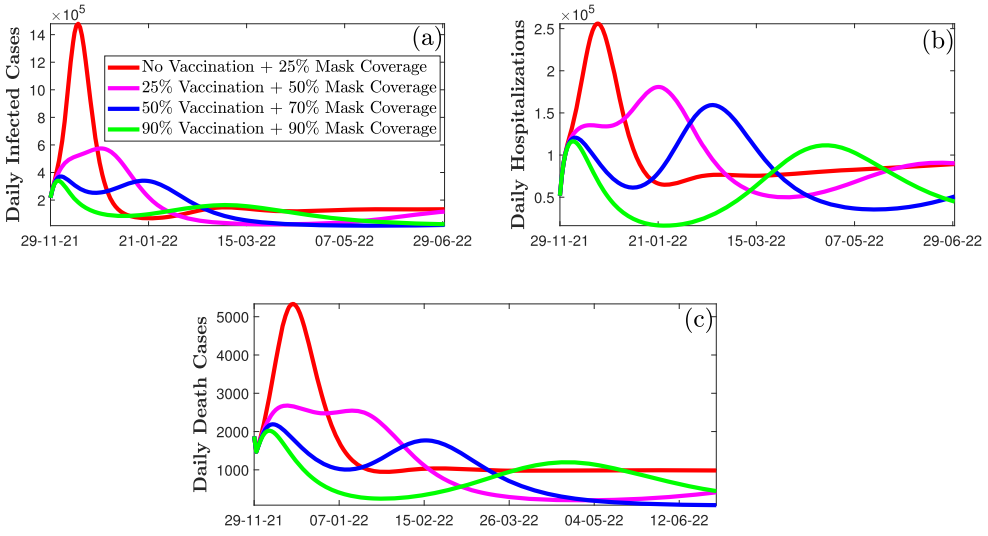

Fig. 14. Simulation of the model (5) showing the combined effect of mask coverage and vaccine coverage. Fig. 14 (a), (b), and (c) show the daily infected cases, daily hospitalized cases, and daily deaths respectively.

original strain. Mathematical analysis was performed to calculate the control reproduction number and to prove the global stability of the DFE when $\mathcal{R}_c < 1$. Vaccine derived herd immunity threshold was then calculated to determine the minimum number of individuals who should be vaccinated to acquire immunity against COVID-19. Then we proved a theorem for the existence of the endemic equilibria. After that, it was shown that there exists a unique endemic equilibrium which is locally asymptotic stable when $\mathcal{R}_j > 1, \quad j = 1, 2, 3$. The model also exhibits backward bifurcation phenomena for all the three strains considered separately when $\mathcal{R}_j < 1, \quad j = 1, 2, 3$. Numerical simulations were carried out to support the theoretical results and to show the effect of Delta and Omicron variants on the dynamics of COVID-19. Numerical results show that whenever a new more contagious variant emerges and becomes dominant, the preexisting variant becomes weak and disappears. It was also observed that due to the emergence of more contagious and potential variants, new waves of COVID-19 arrive which might become more dangerous resulting in more infections and more deaths. This implies that vaccination alone will not be sufficient to eliminate COVID-19. In numerical simulations, the effect of mask coverage with different mask efficacy has also been assessed. But the use of face masks and other non-pharmaceutical interventions can not guarantee the elimination of COVID-19. Again numerical simulations were carried out to assess the impact of vaccines of different efficacy. The results showed that new waves appear after a few days despite the highly effective vaccines being administered. This is happening due to the emergence of Delta and Omicron variants. Since most of the vaccines were designed to

fight against the wild strain, they work efficiently against the original strain but the emergence of new and more dangerous variants weakens their effectiveness. Further numerical simulations were carried out to present the effect of the combination of face masks and vaccines. From the simulation, it was observed that a combination of face masks and vaccines can eliminate the maximum number of daily cases compared to the use of face masks and vaccines alone. Accordingly, the study suggests that a combination of non-pharmaceutical interventions and vaccination programs should be continued to control the disease outbreak.

On the whole, the study found that the presence of both the Delta and Omicron variants along with the original strain almost doubled the number of infections and increased the number of deaths by about 19%. Therefore our study suggests that more dosages of vaccines and new more effective vaccines should be provided in the community to control the new variants.

CRediT authorship contribution statement

Shikha Saha, Amit Kumar Saha: Conceived and designed the experiments; Performed the experiments; Analyzed and interpreted the data; Contributed reagents, materials, analysis tools or data; Wrote the paper.

Funding statement

This research did not receive any specific grant from funding agencies in the public, commercial, or not-for-profit sectors.

Declaration of competing interest

The authors declare no conflict of interest.

Data availability

No data was used for the research described in the article.

Acknowledgements

The authors would like to acknowledge and thank the anonymous editors and reviewers for their helpful comments that have significantly improved this article.

Appendix A. Backward bifurcation for the model with the original strain only

We will discuss the backward bifurcation phenomenon using the Center Manifold theory [37,32]. For this let us consider the changes of variable as $S = x_1$, $V = x_2$, $E_1 = x_3$, $P_1 = x_4$, $I_1 = x_5$, $A_1 = x_6$, $E_2 = 0$, $P_2 = 0$, $I_2 = 0$, $A_2 = 0$, $E_3 = 0$, $P_3 = 0$, $I_3 = 0$, $A_3 = 0$, $Q = x_7$, $H = x_8$ and $R = x_9$, so that in vector form the model (5) can be written as $\frac{dX}{dt} = (f_1, f_2, f_3, f_4, f_5, f_6, f_7, f_8, f_9)^T$, where $X = (x_1, x_2, x_3, x_4, x_5, x_6, x_7, x_8, x_9)^T$ and then we have

$$\begin{aligned}
\frac{dx_1}{dt} &= f_1 = \Lambda + \zeta x_2 + \alpha x_9 - \lambda_1 x_1 - k_1 x_1,\\
\frac{dx_2}{dt} &= f_2 = \rho x_1 - (1-\epsilon_1)\lambda_1 x_2 - k_2 x_2,\\
\frac{dx_3}{dt} &= f_3 = \lambda_1 x_1 + (1-\epsilon_1)\lambda_1 x_2 - k_3 x_3,\\
\frac{dx_4}{dt} &= f_4 = \sigma_1 x_3 - k_4 x_4,\\
\frac{dx_5}{dt} &= f_5 = b\sigma_2 x_4 - k_5 x_5,\\
\frac{dx_6}{dt} &= f_6 = (1-b)\sigma_2 x_4 - k_6 x_6,\\
\frac{dx_7}{dt} &= f_7 = \sigma_q x_6 - k_{11} x_7,\\
\frac{dx_8}{dt} &= f_8 = \phi_{i_1} x_5 + \phi_q x_7 - k_{12} x_8,\\
\frac{dx_9}{dt} &= f_9 = \psi_{i_1} x_5 + \psi_{a_1} x_6 + \psi_q x_7 + \psi_h x_8 - k_{13} x_9.
\end{aligned} \tag{A.1}$$

The Jacobian of the system (A.1) is given by:

$$J(\mathcal{E}_0)=\begin{pmatrix} -k_1 & \zeta & 0 & -\eta_1 J_1 & -J_1 & -\theta_1 J_1 & 0 & 0 & \alpha \\ \rho & -k_2 & 0 & -\eta_1 J_2 & -J_2 & -\theta_1 J_2 & 0 & 0 & 0 \\ 0 & 0 & -k_3 & \eta_1 J_3 & J_3 & \theta_1 J_3 & 0 & 0 & 0 \\ 0 & 0 & \sigma_1 & -k_4 & 0 & 0 & 0 & 0 & 0 \\ 0 & 0 & 0 & b\sigma_2 & -k_5 & 0 & 0 & 0 & 0 \\ 0 & 0 & 0 & (1-b)\sigma_2 & 0 & -k_6 & 0 & 0 & 0 \\ 0 & 0 & 0 & 0 & \sigma_q & 0 & -k_{11} & 0 & 0 \\ 0 & 0 & 0 & 0 & \phi_{i_1} & 0 & \phi_q & -k_{12} & 0 \\ 0 & 0 & 0 & 0 & \psi_{i_1} & \psi_{a_1} & \psi_q & \psi_h & -k_{13} \end{pmatrix},$$

where,

$$J_1 = \frac{(1-em)\beta k_2}{\rho+k_2},\ J_2 = \frac{(1-em)\beta\rho(1-\epsilon_1)}{\rho+k_2},\ \text{and}\ J_3 = \frac{(1-em)\beta\{k_2+\rho(1-\epsilon_1)\}}{\rho+k_2}.$$

Now consider $\mathcal{R}_1=1$ and $\beta_1=\beta_1^*$ is a bifurcation parameter. Thus we get

$$\beta_1 = \beta_1^* = \frac{k_3 k_4 k_5 k_6 N^*}{(1-em)\{S^*+(1-\epsilon_1)V^*\}\sigma_1\{\eta_1 k_5 k_6 + b\sigma_2 k_6 + (1-b)\sigma_2\theta_1 k_5\}}. \tag{A.2}$$

The Jacobian $J(\mathcal{E}_0)$ of (A.1) with $\beta_1=\beta_1^*$ (equation (A.2)), denoted by $J_{\beta_1^*}$, has a simple zero eigenvalue (with all other eigenvalues having negative real part). Hence, the Center Manifold theory [37,32], can be used to analyze the dynamics of the model (5).

Eigenvectors of $J_{\beta_1^*} = J(\mathcal{E}_0)\Big|_{\beta_1=\beta_1^*}$: When $\mathcal{R}_1=1$, the jacobian ($J_{\beta_1^*}$) of (A.1) has a right eigenvector given by $w=[w_1, w_2, w_3, w_4, w_5, w_6, w_7, w_8, w_9]^T$, where,

$$w_1 = w_1,\ w_2 = -\frac{\rho w_1 - \eta_1 j_2 w_4 - j_2 w_5 - \theta_1 j_2 w_6}{k_2},\ w_3 = w_3,\ w_4 = \frac{\sigma_1}{k_4} w_3,\ w_5 = \frac{b\sigma_2}{k_5} w_4,$$
$$w_6 = \frac{(1-b)\sigma_2}{k_6} w_4,\ w_7 = \frac{\sigma_q}{k_{11}} w_5,\ w_8 = \frac{\phi_{i_1} w_5 + \phi_q w_7}{k_{12}},\ w_9 = \frac{\psi_{i_1} w_5 + \psi_{a_1} w_6 + \psi_q w_7 + \psi_h w_8}{k_{13}}.$$

Further, J_{β^*} has a left eigenvector $v=[v_1, v_2, v_3, v_4, v_5, v_6, v_7, v_8, v_9]$, where,

$$v_1 = v_1,\ v_2 = \frac{\zeta}{k_2} v_1,\ v_3 = v_3,\ v_4 = \frac{k_3}{\sigma_1} v_3,\ v_5 = \frac{-J_1 v_1 - J_2 v_2 - J_3 v_3 + \sigma_q v_7 + \phi_{i_1} v_8 + \psi_{i_1} v_9}{k_5},$$
$$v_6 = \frac{-J_1\theta_1 v_1 - J_2\theta_1 v_2 - J_3\theta_1 v_3 + \psi_{a_1} v_9}{k_6},\ v_7 = \frac{\phi_q v_8 + \psi_q v_9}{k_{11}},\ v_8 = \frac{\psi_h}{k_{12}} v_9,\ v_9 = \frac{\alpha}{k_{13}}, v_1.$$

Computations of $a_1\left(a_1 = \sum_{k,i,j=1}^{n} v_k w_i w_j \frac{\partial^2 f_k}{\partial x_i \partial x_j}(\mathcal{E}_0, \beta_1^*)\right)$ and $b_1\left(b_1 = \sum_{k,i=1}^{n} v_k w_i \frac{\partial^2 f_k}{\partial x_i \partial \beta_1}(\mathcal{E}_0, \beta_1^*)\right)$ [37,38]:
After some tedious manipulations, it can be shown that

$$a_1 = -\frac{2\beta_1(1-em)(\rho\zeta - k_1 k_2)(\eta_1 w_4 + \theta_1 w_6 + w_5)}{\Lambda(\rho+k_2)^2}\Bigg[\Big\{w_6 k_2 v_1 - w_8 k_2 v_3 - k_2 v_3 w_3 + w_7 k_2 v_1 + w_9 k_2 v_1$$
$$+ w_4 k_2 v_1 - w_6 k_2 v_3 - k_2 v_3 w_2 - w_4 k_2 v_3 + k_2 v_1 w_3 + w_8 k_2 v_1 + k_2 v_1 w_1 - w_9 k_2 v_3 - w_7 k_2 v_3 - \rho v_1 w_1$$
$$+ \rho v_3 w_1 - v_3 w_3 k_2 + v_1 w_5 k_2 + (1-\epsilon_1)\Big(v_2 w_5 \rho - v_3 w_5 \rho + \rho w_4 v_2 - \rho w_6 v_2 - \rho w_6 v_3 + \rho w_7 v_2$$
$$- \rho w_7 v_3 + \rho w_8 v_2 - \rho w_8 v_3 + \rho w_9 v_2 - \rho w_9 v_3 + \rho v_2 w_1 + \rho v_2 w_3 - \rho v_3 w_1 - \rho v_3 w_3 - k_2 v_2 w_2 + k_2 v_3 w_2\Big)\Big\}\Bigg],$$

$$\text{and } b_1 = -\frac{(1-em)(\eta_1 w_4 + \theta_1 w_6 + w_5)\Big((1-\epsilon_1)\rho(v_2 - v_3) + k_2 v_1 - k_2 v_3\Big)}{\rho + k_2}. \tag{A.3}$$

Appendix B. Proof of the global stability of the DFE for the model (Theorem 12))

Proof. To prove the global stability of the DFE, we consider the following linear Lyapunov function:

$$\mathcal{L}_1 = \ell_1 E_1 + \ell_2 P_1 + \ell_3 I_1 + \ell_4 A_1,$$

where,

$$\ell_1 = \frac{\eta_1\sigma_1}{k_3 k_4} + \frac{b\sigma_1\sigma_2}{k_3 k_4 k_5} + \frac{\theta_1(1-b)\sigma_1\sigma_2}{k_3 k_4 k_6},\ \ell_2 = \frac{k_3}{\sigma_1}\ell_1,\ \ell_3 = \frac{1}{k_5},\ \ell_4 = \frac{\theta_1}{k_6}.$$

Differentiating the above Lyapunov function we have the following

$$\begin{aligned}\dot{\mathcal{L}}_1 &= \ell_1 \dot{E}_1 + \ell_2 \dot{P}_1 + \ell_3 \dot{I}_1 + \ell_4 \dot{A}_1 \\ &= \ell_1 \left\{ \lambda_1 (S + (1-\epsilon_1)V) - k_3 E_1 \right\} + \ell_2 (\sigma_1 E_1 - k_4 P_1) + \ell_3 (b\sigma_2 P_1 - k_5 I_1) + \ell_4 \left\{ (1-b)\sigma_2 P_1 - k_6 A_1 \right\}\end{aligned}$$

After some rigorous calculations, it can be shown that

$$\dot{\mathcal{L}}_1 \leq (\eta_1 P_1 + I_1 + \theta_1 A_1)(\mathcal{R}_1 - 1). \tag{B.1}$$

Again consider

$$\mathcal{L}_2 = \ell_5 E_2 + \ell_6 P_2 + \ell_7 I_2 + \ell_8 A_2,$$

where,

$$\ell_5 = \frac{\eta_2\sigma_1}{k_3 k_4} + \frac{b\sigma_1\sigma_2}{k_3 k_4 k_7} + \frac{\theta_2(1-b)\sigma_1\sigma_2}{k_3 k_4 k_8},\ \ell_6 = \frac{k_3}{\sigma_1}\ell_5,\ \ell_7 = \frac{1}{k_7},\ \ell_8 = \frac{\theta_2}{k_8}.$$

Differentiating the above Lyapunov function we have the following

$$\begin{aligned}\dot{\mathcal{L}}_2 &= \ell_5 \dot{E}_2 + \ell_6 \dot{P}_2 + \ell_7 \dot{I}_2 + \ell_8 \dot{A}_2 \\ &= \ell_5 \left\{ \lambda_2 (S + (1-\epsilon_2)V) - k_3 E_2 \right\} + \ell_6 (\sigma_1 E_2 - k_4 P_2) + \ell_7 (b\sigma_2 P_2 - k_7 I_2) + \ell_8 \left\{ (1-b)\sigma_2 P_2 - k_8 A_2 \right\}\end{aligned}$$

After some rigorous calculations, it can be shown that

$$\dot{\mathcal{L}}_2 \leq (\eta_2 P_2 + I_2 + \theta_2 A_2)(\mathcal{R}_2 - 1). \tag{B.2}$$

Again consider

$$\mathcal{L}_3 = \ell_9 E_3 + \ell_{10} P_3 + \ell_{11} I_3 + \ell_{12} A_3,$$

where,

$$\ell_9 = \frac{\eta_3\sigma_1}{k_3 k_4} + \frac{b\sigma_1\sigma_2}{k_3 k_4 k_9} + \frac{\theta_3(1-b)\sigma_1\sigma_2}{k_3 k_4 k_{10}},\ \ell_{10} = \frac{k_3}{\sigma_1}\ell_9,\ \ell_{11} = \frac{1}{k_9},\ \ell_{11} = \frac{\theta_3}{k_{10}}.$$

Differentiating the above Lyapunov function we have the following

$$\begin{aligned}\dot{\mathcal{L}}_3 &= \ell_9 \dot{E}_3 + \ell_{10} \dot{P}_3 + \ell_{11} \dot{I}_3 + \ell_{12} \dot{A}_3 \\ &= \ell_9 \left\{ \lambda_3 (S + (1-\epsilon_3)V) - k_3 E_3 \right\} + \ell_{10} (\sigma_1 E_3 - k_4 P_3) + \ell_{11} (b\sigma_2 P_3 - k_9 I_3) + \ell_{12} \left\{ (1-b)\sigma_2 P_3 - k_{10} A_3 \right\}\end{aligned}$$

After some calculations, it can be shown that

$$\dot{\mathcal{L}}_3 \leq (\eta_3 P_3 + I_3 + \theta_3 A_3)(\mathcal{R}_3 - 1). \tag{B.3}$$

Hence, adding (B.1), (B.2), and (B.3) we get

$$\dot{\mathcal{L}}_1 + \dot{\mathcal{L}}_2 + \dot{\mathcal{L}}_3 \leq (\eta_1 P_1 + I_1 + \theta_1 A_1)(\mathcal{R}_1 - 1) + (\eta_2 P_2 + I_2 + \theta_2 A_2)(\mathcal{R}_2 - 1) + (\eta_3 P_3 + I_3 + \theta_3 A_3)(\mathcal{R}_3 - 1).$$

Let $\mathcal{R}_c = \max\{\mathcal{R}_1, \mathcal{R}_2, \mathcal{R}_3\}$

Thus

$$\dot{\mathcal{L}} = \dot{\mathcal{L}}_1 + \dot{\mathcal{L}}_2 + \dot{\mathcal{L}}_3 \leq N^*(\lambda_1 + \lambda_2 + \lambda_3)(\mathcal{R}_c - 1) \leq 0 \quad \text{for} \quad \mathcal{R}_c \leq 1. \tag{B.4}$$

Also $\dot{\mathcal{L}} = 0$ if and only if $E_j = P_j = I_j = A_j = 0$, $j = 1, 2, 3$. Hence $\dot{\mathcal{L}} \leq 0$ (from (B.4)). Therefore, $\mathcal{L}$ is a Lyapunov function on $\mathcal{D}$ and thus it follows by the LaSalle's invariance principle [43] that, the DFE of the model (5) is globally asymptotic stable whenever $\mathcal{R}_c \leq 1$.

Appendix C. Endemic equilibria and backward bifurcation of the model with the original strain and the Delta variant

Let $\mathcal{E}_2 = (S^*, V^*, 0, 0, 0, 0, E_2^*, P_2^*, I_2^*, A_2^*, 0, 0, 0, 0, Q^*, H^*, R^*)$ be any arbitrary equilibrium of the model (5) with the original strain and the Delta variant and hence equation (3) can be written as

$$\lambda_2^* = \frac{\beta_2(1 - e\,m)(\eta_2 P_2^* + I_2^* + \theta_2 A_2^*)}{N^*} \tag{C.1}$$

be the force of infection at steady-state. Therefore, from the system (29) we have,

$$\begin{aligned}S^* &= \frac{\Lambda k_3 \left\{ (1-\epsilon_2)\lambda_2^* + k_2 \right\}}{M_{1_2}\lambda_2^{*^2} + M_{2_2}\lambda_2^* + M_{3_2}},\quad V^* = \frac{\rho\Lambda k_3}{M_{1_2}\lambda_2^{*^2} + M_{2_2}\lambda_2^* + M_{3_2}},\quad E_2^* = \frac{\lambda_2^*(M_{4_2}\lambda_2^* + M_{5_2})}{M_{1_2}\lambda_2^{*^2} + M_{2_2}\lambda_2^* + M_{3_2}}, \\ P_2^* &= B_{p_2} E_2^*,\quad I_2^* = B_{i_2} E_2^*,\quad A_2^* = B_{a_2} E_2^*,\quad Q^* = B_{q_2} E_2^*,\quad H^* = B_{h_2} E_2^*,\quad R^* = B_{r_2} E_2^*,\end{aligned} \tag{C.2}$$

where,

$$B_{p_2} = \frac{\sigma_1}{k_4},\ B_{i_2} = \frac{b\sigma_2}{k_7},\ B_{a_2} = \frac{(1-b)\sigma_2}{k_8},\ B_{q_2} = \frac{b\sigma_1\sigma_2\sigma_q}{k_4 k_7 k_{11}},\ B_{h_2} = \frac{\phi_{i_2} B_{i_2} + \phi_q B_{q_2}}{k_{12}},$$
$$B_{r_2} = \frac{\psi_{i_2} B_{i_2} + \psi_{a_2} B_{a_2} + \psi_q B_{q_2} + \psi_h B_{h_2}}{k_{13}},\ M_{1_2} = (1-\epsilon_2)(k_3 + \alpha B_{r_2}),\ M_{2_2} = (1-\epsilon_2)k_1 k_3 + k_2(1-\alpha B_{r_2}) - \alpha B_{r_2}(1-\epsilon_2)\rho,$$
$$M_{3_2} = -\eta\rho k_2,\ M_{4_2} = \Lambda(1-\epsilon_2),\ M_{5_2} = \Lambda k_2 + \Lambda(1-\epsilon_2)\rho.$$

Substituting (C.2) into (C.1) gives

$$\lambda_2^* = \frac{\beta_2(1-em)(\eta_2 B_{p_2} + B_{i_2} + \theta_2 B_{a_2})\left(M_{4_2}\lambda_2^{*2} + M_{5_2}\lambda_2^*\right)}{\Lambda k_3\left\{(1-\epsilon_2)\lambda_2^* + k_2\right\} + \rho\Lambda k_3 + B_{c_2}\left(M_{4_2}\lambda_2^{*2} + M_{5_2}\lambda_2^*\right)}, \tag{C.3}$$

where,

$$B_{c_2} = 1 + B_{p_2} + B_{i_2} + B_{a_2} + B_{q_2} + B_{h_2} + B_{r_2}.$$

After some algebraic calculation, the following polynomial equation in terms of λ_2^* can be obtained from equation (C.3) as

$$\lambda_2^*\left\{P_{2_2}\lambda_2^{*2} + P_{1_2}\lambda_2^* + P_{0_2}\right\} = 0, \tag{C.4}$$

where,

$$\begin{aligned} P_{2_2} &= B_{c_2} M_{4_2}, \\ P_{1_2} &= B_{c_2} M_{5_2} + \Lambda k_3(1-\epsilon_2) - M_{4_2}\beta_2(1-em)(\eta_2 B_{p_2} + B_{i_2} + \theta_2 B_{a_2}), \\ P_{0_2} &= \Lambda k_3(\rho + k_2)(1-\mathcal{R}_2). \end{aligned} \tag{C.5}$$

Out of the three roots, the root $\lambda_2^* = 0$, of (C.4), corresponds to the DFE $\mathcal{E}_0$. Equation (C.4) says that the non-zero equilibria of the model satisfy

$$f(\lambda_2^*) = P_{2_2}\lambda_2^{*2} + P_{1_2}\lambda_2^* + P_{0_2} = 0. \tag{C.6}$$

Using Theorem 5 and following the same procedure as in Appendix A, it can be shown that the expressions of a_2 and b_2 for the original model with Delta variant are

$$\begin{aligned} a_2 = &-\frac{2\beta_2(1-em)(\rho\zeta - k_1 k_2)(\eta_1 w_4 + \theta_1 w_6 + w_5)}{\Lambda(\rho + k_2)^2}\Bigg[\Big\{w_6 k_2 v_1 - w_8 k_2 v_3 - k_2 v_3 w_3 + w_7 k_2 v_1 + w_9 k_2 v_1 \\ &+ w_4 k_2 v_1 - w_6 k_2 v_3 - k_2 v_3 w_2 - w_4 k_2 v_3 + k_2 v_1 w_3 + w_8 k_2 v_1 + k_2 v_1 w_1 - w_9 k_2 v_3 - w_7 k_2 v_3 \\ &- \rho v_1 w_1 + \rho v_3 w_1 - v_3 w_3 k_2 + v_1 w_5 k_2 + (1-\epsilon_2)\Big(v_2 w_5 \rho - v_3 w_5 \rho + \rho w_4 v_2 - \rho w_6 v_2 - \rho w_6 v_3 \\ &+ \rho w_7 v_2 - \rho w_7 v_3 + \rho w_8 v_2 - \rho w_8 v_3 + \rho w_9 v_2 - \rho w_9 v_3 + \rho v_2 w_1 + \rho v_2 w_3 - \rho v_3 w_1 - \rho v_3 w_3 \\ &- k_2 v_2 w_2 + k_2 v_3 w_2\Big)\Big\}\Bigg], \\ \text{and } b_2 = &-\frac{(1-em)(\eta_1 w_4 + \theta_1 w_6 + w_5)\Big((1-\epsilon_2)\rho(v_2 - v_3) + k_2 v_1 - k_2 v_3\Big)}{\rho + k_2}. \end{aligned} \tag{C.7}$$

Appendix D. Endemic equilibria and backward bifurcation of the model with the original strain and the Delta and Omicron variants

Let $\mathcal{E}_3 = (S^*, V^*, 0, 0, 0, 0, 0, 0, 0, 0, E_3^*, P_3^*, I_3^*, A_3^*, Q^*, H^*, R^*)$ be any arbitrary equilibrium of the model (5) with the original strain and the Delta and Omicron variants and hence equation (4) can be written as

$$\lambda_3^* = \frac{\beta_3(1-em)(\eta_3 P_3^* + I_3^* + \theta_3 A_3^*)}{N^*} \tag{D.1}$$

be the force of infection at steady-state. Therefore, from the system (29) we have,

$$\begin{aligned} S^* &= \frac{\Lambda k_3\left\{(1-\epsilon_3)\lambda_2^* + k_2\right\}}{M_{1_2}\lambda_2^{*2} + M_{2_2}\lambda_2^* + M_{3_2}},\quad V^* = \frac{\rho\Lambda k_3}{M_{1_3}\lambda_3^{*2} + M_{2_3}\lambda_2^* + M_{3_3}},\quad E_3^* = \frac{\lambda_2^*(M_{4_3}\lambda_3^* + M_{5_3})}{M_{1_3}\lambda_3^{*2} + M_{2_3}\lambda_3^* + M_{3_3}}, \\ P_3^* &= B_{p_3} E_3^*,\ I_3^* = B_{i_3} E_3^*,\ A_3^* = B_{a_3} E_3^*,\ Q^* = B_{q_3} E_3^*,\ H^* = B_{h_3} E_3^*,\ R^* = B_{r_3} E_3^*, \end{aligned} \tag{D.2}$$

where,

$$B_{p_3} = \frac{\sigma_1}{k_4},\ B_{i_3} = \frac{b\sigma_2}{k_9},\ B_{a_3} = \frac{(1-b)\sigma_2}{k_{10}},\ B_{q_3} = \frac{b\sigma_1\sigma_2\sigma_q}{k_4 k_9 k_{11}},\ B_{h_3} = \frac{\phi_{i_3} B_{i_3} + \phi_q B_{q_3}}{k_{12}},$$

$$B_{r_3} = \frac{\psi_{i_3} B_{i_3} + \psi_{a_3} B_{a_3} + \psi_q B_{q_3} + \psi_h B_{h_3}}{k_{13}},\ M_{1_3} = (1-\epsilon_3)(k_3 + \alpha B_{r_3}),\ M_{2_3} = (1-\epsilon_3)k_1 k_3 + k_2(1-\alpha B_{r_3}) - \alpha B_{r_3}(1-\epsilon_3)\rho,$$

$$M_{3_3} = -\eta\rho k_2,\ M_{4_3} = \Lambda(1-\epsilon_3),\ M_{5_3} = \Lambda k_2 + \Lambda(1-\epsilon_3)\rho.$$

Substituting (D.2) into (D.1) gives

$$\lambda_3^* = \frac{\beta_3(1-e\,m)(\eta_3 B_{p_3} + B_{i_3} + \theta_3 B_{a_3})\left(M_{4_3}\lambda_3^{*2} + M_{5_3}\lambda_3^*\right)}{\Lambda k_3\left\{(1-\epsilon_3)\lambda_3^* + k_2\right\} + \rho\Lambda k_3 + B_{c_3}\left(M_{4_3}\lambda_3^{*2} + M_{5_3}\lambda_3^*\right)}, \tag{D.3}$$

where,

$$B_{c_3} = 1 + B_{p_3} + B_{i_3} + B_{a_3} + B_{q_3} + B_{h_3} + B_{r_3}.$$

After some algebraic calculation, the following polynomial equation in terms of λ_3^* can be obtained from equation (D.3) as

$$\lambda_3^*\left\{P_{2_3}\lambda_3^{*2} + P_{1_3}\lambda_3^* + P_{0_3}\right\} = 0, \tag{D.4}$$

where,

$$\begin{aligned} P_{2_3} &= B_{c_3} M_{4_3}, \\ P_{1_3} &= B_{c_3} M_{5_3} + \Lambda k_3(1-\epsilon_3) - M_{4_3}\beta_3(1-e\,m)(\eta_3 B_{p_3} + B_{i_3} + \theta_3 B_{a_3}), \\ P_{0_3} &= \Lambda k_3(\rho + k_3)(1-\mathcal{R}_3). \end{aligned} \tag{D.5}$$

Out of the three roots, the root $\lambda_3^* = 0$, of (D.4), corresponds to the DFE $\mathcal{E}_0$. Equation (D.4) says that the non-zero equilibria of the model satisfy

$$f(\lambda_3^*) = P_{2_3}\lambda_3^{*2} + P_{1_3}\lambda_3^* + P_{0_3} = 0. \tag{D.6}$$

Using Theorem 9 and following the same procedure as in Appendix A, it can be shown that the expressions of a_3 and b_3 for the original model with Delta and Omicron variants are

$$\begin{aligned} a_3 = -\frac{2\beta_3(1-e\,m)(\rho\eta - k_1 k_2)(\eta_3 w_4 + \theta_3 w_6 + w_5)}{\Lambda(\rho + k_2)^2}\Bigg[\Big\{ & w_6 k_2 v_1 - w_8 k_2 v_3 - k_2 v_3 w_3 + w_7 k_2 v_1 + w_9 k_2 v_1 \\ & + w_4 k_2 v_1 - w_6 k_2 v_3 - k_2 v_3 w_2 - w_4 k_2 v_3 + k_2 v_1 w_3 + w_8 k_2 v_1 + k_2 v_1 w_1 - w_9 k_2 v_3 - w_7 k_2 v_3 \\ & - \rho v_1 w_1 + \rho v_3 w_1 - v_3 w_3 k_2 + v_1 w_5 k_2 + (1-\epsilon_3)\Big(v_2 w_5\rho - v_3 w_5\rho + \rho w_4 v_2 - \rho w_6 v_2 - \rho w_6 v_3 + \rho w_7 v_2 \\ & - \rho w_7 v_3 + \rho w_8 v_2 - \rho w_8 v_3 + \rho w_9 v_2 - \rho w_9 v_3 + \rho v_2 w_1 + \rho v_2 w_3 - \rho v_3 w_1 - \rho v_3 w_3 - k_2 v_2 w_2 + k_2 v_3 w_2\Big)\Big\}\Bigg], \\ \text{and } b_3 = -\frac{(1-e\,m)(\eta_3 w_4 + \theta_3 w_6 + w_5)\Big((1-\epsilon_3)\rho(v_2 - v_3) + k_2 v_1 - k_2 v_3\Big)}{\rho + k_2}. \end{aligned} \tag{D.7}$$

References

[1] Center for Disease Control and Prevention, About-Covid-19, basics-Covid-19, https://www.cdc.gov/coronavirus/2019-ncov/your-health/about-covid-19/basics-covid-19.html. (Accessed 22 June 2022).

[2] Worldometers-coronavirus-daily-information, https://www.worldometers.info/coronavirus/. (Accessed 15 March 2023).

[3] S. Moore, E.M. Hill, M.J. Tildesley, L. Dyson, M.J. Keeling, Vaccination and non-pharmaceutical interventions for Covid-19: a mathematical modelling study, Lancet Infect. Dis. 21 (6) (2021) 793–802, https://doi.org/10.1016/S1473-3099(21)00143-2.

[4] Coronavirus, prevention-and-control, non-pharmaceutical-interventions, https://www.ecdc.europa.eu/en/covid-19/prevention-and-control/non-pharmaceutical-interventions. (Accessed 25 July 2022).

[5] C.N. Ngonghala, E.A. Iboi, A.B. Gumel, Could masks curtail the post-lockdown resurgence of Covid-19 in the US?, Math. Biosci. 329 (2020) 108452, https://doi.org/10.1016/j.mbs.2020.108452.

[6] A.K. Saha, C.N. Podder, A.M. Niger, Dynamics of novel Covid-19 in the presence of co-morbidity, Infect. Dis. Model. 7 (2) (2022) 138–160, https://doi.org/10.1016/j.idm.2022.04.005.

[7] World health organization, Covid-19-vaccine-eul-issued, https://extranet.who.int/pqweb/vaccines/vaccinescovid-19-vaccine-eul-issued. (Accessed 15 May 2022).

[8] Center for Disease Control and Prevention, Coronavirus, variants, about-variants, https://www.cdc.gov/coronavirus/2019-ncov/variants/about-variants.html. (Accessed 10 June 2022).

[9] Coronavirus, disease-and-conditions, variant-of-concerns, https://www.publichealthontario.ca/en/diseases-and-conditions/infectious-diseases/respiratory-diseases/novel-coronavirus/variants. (Accessed 25 June 2022).

[10] Center for Disease Control and Prevention, Coronavirus, variants, variant-classifications, https://www.cdc.gov/coronavirus/2019-ncov/variants/variant-classifications.html. (Accessed 15 July 2022).

[11] N.G. Davies, S. Abbott, R.C. Barnard, C.I. Jarvis, A.J. Kucharski, J.D. Munday, C.A. Pearson, T.W. Russell, D.C. Tully, A.D. Washburne, et al., Estimated transmissibility and impact of Sars-CoV-2 lineage b. 1.1. 7 in England, Science 372 (6538) (2021) eabg3055, https://doi.org/10.1126/science.abg3055.
[12] P. Mlcochova, S.A. Kemp, M.S. Dhar, G. Papa, B. Meng, I.A. Ferreira, R. Datir, D.A. Collier, A. Albecka, S. Singh, et al., Sars-CoV-2 B.1.617. 2 Delta variant replication and immune evasion, Nature 599 (7883) (2021) 114–119, https://doi.org/10.1038/s41586-021-03944-y.
[13] C. Del Rio, S.B. Omer, P.N. Malani, Winter of Omicron - the evolving Covid-19 pandemic, JAMA 327 (4) (2022) 319–320, https://doi.org/10.1001/jama.2021.24315.
[14] E. Callaway, H. Ledford, et al., How bad is Omicron? What scientists know so far, Nature 600 (7888) (2021) 197–199, https://doi.org/10.1038/d41586-021-03614-z.
[15] S.M. Moghadas, T.N. Vilches, K. Zhang, C.R. Wells, A. Shoukat, B.H. Singer, L.A. Meyers, K.M. Neuzil, J.M. Langley, M.C. Fitzpatrick, et al., The impact of vaccination on coronavirus disease 2019 (Covid-19) outbreaks in the United States, Clin. Infect. Dis. 73 (12) (2021) 2257–2264, https://doi.org/10.1093/cid/ciab079.
[16] M. Mancuso, S.E. Eikenberry, A.B. Gumel, Will vaccine-derived protective immunity curtail Covid-19 variants in the us?, Infect. Dis. Model. 6 (2021) 1110–1134, https://doi.org/10.1016/j.idm.2021.08.008.
[17] A.K. Saha, S. Saha, C.N. Podder, Effect of awareness, quarantine and vaccination as control strategies on Covid-19 with co-morbidity and re-infection, Infect. Dis. Model. (2022), https://doi.org/10.1016/j.idm.2022.09.004.
[18] B. Ivorra, M.R. Ferrández, M. Vela-Pérez, A.M. Ramos, Mathematical modeling of the spread of the coronavirus disease 2019 (Covid-19) taking into account the undetected infections. The case of China, Commun. Nonlinear Sci. Numer. Simul. 88 (2020) 105303, https://doi.org/10.1016/j.cnsns.2020.105303.
[19] A.J. Kucharski, T.W. Russell, C. Diamond, Y. Liu, J. Edmunds, S. Funk, R.M. Eggo, F. Sun, M. Jit, J.D. Munday, et al., Early dynamics of transmission and control of Covid-19: a mathematical modelling study, Lancet Infect. Dis. 20 (5) (2020) 553–558, https://doi.org/10.1016/S1473-3099(20)30144-4.
[20] K. Mizumoto, G. Chowell, Transmission potential of the novel coronavirus (Covid-19) onboard the diamond princess cruises ship, 2020, Infect. Dis. Model. 5 (2020) 264–270, https://doi.org/10.1016/j.idm.2020.02.003.
[21] N.M. Ferguson, D. Laydon, G. Nedjati-Gilani, N. Imai, K. Ainslie, M. Baguelin, S. Bhatia, A. Boonyasiri, Z. Cucunubá, G. Cuomo-Dannenburg, et al., Impact of non-pharmaceutical interventions (npis) to reduce Covid-19 mortality and healthcare demand, Imperial College Covid-19 Response, Imperial College Covid-19 Response Team, 2020.
[22] D. Okuonghae, A. Omame, Analysis of a mathematical model for Covid-19 population dynamics in Lagos, Nigeria, Chaos Solitons Fractals 139 (2020) 110032, https://doi.org/10.1016/j.chaos.2020.110032.
[23] F.A. Rihan, U. Kandasamy, N. Sottocornola, M.-N. Anwar, A.Q. Khaliq, Stability and bifurcation analysis of the Caputo fractional-order asymptomatic Covid-19 model with multiple time-delays, Int. J. Bifurc. Chaos 33 (02) (2023) 2350022, https://doi.org/10.1142/S0218127423500220.
[24] F.A. Rihan, U. Kandasamy, H.J. Alsakaji, N. Sottocornola, Dynamics of a fractional-order delayed model of Covid-19 with vaccination efficacy, Vaccines 11 (4) (2023) 758, https://doi.org/10.3390/vaccines11040758.
[25] E.F. Arruda, S.S. Das, C.M. Dias, D.H. Pastore, Modelling and optimal control of multi strain epidemics, with application to Covid-19, PLoS ONE 16 (9) (2021) e0257512, https://doi.org/10.1371/journal.pone.0257512.
[26] G. González-Parra, A.J. Arenas, Qualitative analysis of a mathematical model with presymptomatic individuals and two Sars-CoV-2 variants, Comput. Appl. Math. 40 (6) (2021) 1–25, https://doi.org/10.1007/s40314-021-01592-6.
[27] U.A.P. de León, E. Avila-Vales, K.L. Huang, Modeling Covid-19 dynamic using a two-strain model with vaccination, Chaos Solitons Fractals 157 (2022) 111927, https://doi.org/10.1016/j.chaos.2022.111927.
[28] S. Tchoumi, H. Rwezaura, J. Tchuenche, Dynamic of a two-strain Covid-19 model with vaccination, Results Phys. (2022) 105777, https://doi.org/10.1016/j.rinp.2022.105777.
[29] L.J. Akinbami, B.J. Biggerstaff, P.A. Chan, E. McGibbon, P. Pathela, L.R. Petersen, Reinfection with severe acute respiratory syndrome coronavirus 2 among previously infected healthcare personnel and first responders, Clin. Infect. Dis. (2021), https://doi.org/10.1093/cid/ciab952.
[30] Center for Disease Control and Prevention, Coronavirus, reinfection, https://www.cdc.gov/coronavirus/2019-ncov/your-health/reinfection.html. (Accessed 15 May 2022).
[31] O. Diekmann, J.A.P. Heesterbeek, J.A. Metz, On the definition and the computation of the basic reproduction ratio r_0 in models for infectious diseases in heterogeneous populations, J. Math. Biol. 28 (4) (1990) 365–382, https://doi.org/10.1007/BF00178324.
[32] P. Van den Driessche, J. Watmough, Reproduction numbers and sub-threshold endemic equilibria for compartmental models of disease transmission, Math. Biosci. 180 (1–2) (2002) 29–48, https://doi.org/10.1016/S0025-5564(02)00108-6.
[33] C. Castillo-Chavez, Z. Feng, W. Huang, On the computation of R0 and its role on global stability, in: Mathematical Approaches for Emerging and Re-Emerging Infection Diseases: An Introduction, vol. 125, 2002, pp. 31–65.
[34] H.W. Hethcote, The mathematics of infectious diseases, SIAM Rev. 42 (4) (2000) 599–653, https://doi.org/10.1137/S003614450037190.
[35] C.N. Ngonghala, H.B. Taboe, S. Safdar, A.B. Gumel, Unraveling the dynamics of the Omicron and Delta variants of the 2019 coronavirus in the presence of vaccination, mask usage, and antiviral treatment, Appl. Math. Model. 114 (2023) 447–465, https://doi.org/10.1016/j.apm.2022.09.017.
[36] C.N. Ngonghala, E. Iboi, S. Eikenberry, M. Scotch, C.R. MacIntyre, M.H. Bonds, A.B. Gumel, Mathematical assessment of the impact of non-pharmaceutical interventions on curtailing the 2019 novel coronavirus, Math. Biosci. 325 (2020) 108364, https://doi.org/10.1016/j.mbs.2020.108364.
[37] J. Carr, Applications of Centre Manifold Theory, vol. 35, Springer Science & Business Media, 2012.
[38] C. Castillo-Chavez, B. Song, Dynamical models of tuberculosis and their applications, Math. Biosci. Eng. 1 (2) (2004) 361, https://doi.org/10.3934/mbe.2004.1.361.
[39] M. Sanchez, S. Blower, Uncertainty and sensitivity analysis of the basic reproductive rate: tuberculosis as an example, Am. J. Epidemiol. 145 (1997) 1127–1137, https://doi.org/10.1093/oxfordjournals.aje.a009076.
[40] S. Marino, I.B. Hogue, C.J. Ray, D.E. Kirschner, A methodology for performing global uncertainty and sensitivity analysis in systems biology, J. Theor. Biol. 254 (1) (2008) 178–196, https://doi.org/10.1016/j.jtbi.2008.04.011.
[41] S.M. Blower, H. Dowlatabadi, Sensitivity and uncertainty analysis of complex models of disease transmission: an HIV model, as an example, Int. Stat. Rev./Rev. Int. Stat. (1994) 229–243, https://doi.org/10.2307/1403510.
[42] R. Taylor, Interpretation of the correlation coefficient: a basic review, J. Diag. Med. Sonogr. 6 (1) (1990) 35–39, https://doi.org/10.1177/875647939000600106.
[43] J.P. LaSalle, The Stability of Dynamical Systems, SIAM, 1976.